POLITECNICO DI TORINO

Master Degree course in Nanotechnology for ICTs

Master Degree Thesis

Chemical Functionalization and Device Characterization of Nano-scale Field-Effect-Transistors (FETs) for Biomolecule Sensing

Supervisors
Prof. Carlo Ricciardi
Dr. Sybren Santermans

Candidate
Giada Romano

Academic Year 2022-2023

Al mio caro maestro di vita, Antonio.

Abstract

Biosensors have been developed since decades and for a wide range of applications, such as diagnostics, monitoring of diseases, drug discovery and food industry. One key demand for all the different fields is the highly specific detection of biomolecules. Various biosensing strategies have been investigated to obtain more sensitive and specific biological sensors. So far, the most interesting results in terms of low detection limit have been achieved with bottom-up fabricated biosensors. A bottom-up approach allows for more easy and economical fabrication of sensors for proof-of-concept studies compared to the photolithographic process which relies on a cleanroom. However, a top-down photolithographic approach remains the only choice to realize high-volume biosensor chips for high-throughput applications with good yield and reliability. For this reason, this thesis work is focused on the realization of Biological Field-Effect Transistor (bioFET) sensors fabricated in imec's facilities. The established finFET technology process at imec is followed by a metal gate removal step forming a cavity and exposing the gate oxide to the environment. Afterward, the oxide surface is functional with a self-assembled monolayer (SAM) to obtain a biosensor that is specific to a certain target biomolecule. The use of the advanced silicon-based finFET technology allows for high-density integration and parallelization of bioFETs on chip. Moreover, finFETs can be made small while still maintaining good electrical parameters, which is critical to achieve the single-molecule detection limit with bioFET sensors. When biomolecules attach to the FET's surface, the channel charge is redistributed and so a modulation of the FET drain current occurs. The molecule signal depends strongly on the nature of the bioFET's surface. For this reason, two types of aminoalkylsilane SAMs have been characterized: 3-Aminopropyltrimethoxysilane (APTMS) and 11-aminoundecyltriethoxysilane (AUTES). The two functional layers have been characterized in terms of contact angle, thickness, surface charge and binding capability. Consistent results have been obtained for the different surface characterization techniques. Afterwards, the best SAM has been deposited on the bioFETs to proceed with the electrical characterization. At this stage, the good quality of the devices has been demonstrated in terms of electrical parameters like threshold voltage and subthreshold swing. These parameters have been compared with ideal values found in literature and with experimental results derived by previous works. The aminoalkylsilane functionalized bioFETs give subthreshold swing values like the uncoated devices. This means that the functional layer does not impede the good functioning of the FETs. The electrical characterization ends with the two-step binding of 2μM 50A50T DNA oligonucleotides to the bioFET surface using glutaraldehyde as a cross-linker. The experiments show a clear change in the FET current after the binding of glutaraldehyde with the aminoalkylsilane functional layer. However, the injection of DNA in the flow cell does not result in a DNA signal. Outcomes and possible reasons behind the results are analysed and discussed at the end of the electrical characterization part. Eventually, limitations of the presented study and outlook on biomolecule detection with silicon-based FETs will conclude the thesis.

Sommario

I biosensori vengono sviluppati da decenni e per una vasta gamma di applicazioni, tra cui diagnostica, monitoraggio delle malattie, scoperta di nuovi farmaci e industria alimentare. Una richiesta chiave comune a tutti questi campi di applicazione è l'alta specificità nella rilevazione delle biomolecole. A tale scopo, varie strategie sono state studiate per ottenere sensori sempre più sensibili e specifici alla rilevazione di agenti biologici. Fino ad oggi, i risultati più interessanti riguardanti sensori con un basso limite di rilevamento sono stati raggiunti seguendo il cosiddetto approccio botton-up. Tale approccio, se comparato ai classici processi litografici adottati nelle camere bianche, garantisce una fabbricazione più semplice ed economica. Tuttavia, la sua applicazione è limitata a dimostrazioni di fattibilità e non espandibile ad applicazioni ad alta produttività. Perciò, il processo opposto, cosidetto approccio top-down, rimane l'unica scelta possibile per realizzare un volume elevato di dispositivi con un buon rendimento e un'adeguata affidabilità. Per questo motivo, il seguente lavoro di tesi è incentrato sulla realizzazione di biosensori basati su transistors ad effetto di campo (FETs) interamente prodotti in imec. La produzione di tali dispositivi è basata sulla tecnologia finFET che viene ultimata attraverso un processo di fabbricazione ben consolidato ad imec. Dopo di che, al processo standard di produzione si aggiunge la rimozione del metallo di gate col fine di formare una cavità dove l'ossido di gate viene esposto all'ambiente esterno. Successivamente, la superficie ossidata è funzionalizzata attraverso la creazione di un monostrato auto-assemblato (SAM) in modo da ottenere un biosensore che sia specifico ad una certa molecola bersaglio. L'utilizzo di una tecnologia molto avanzata e basata sul silicio come la tecnologia finFET, garantisce il raggiungimento di un'elevata integrazione e parallelizzazione di transistors all'interno di un unico chip. Inoltre, i transistors fabbricati con la tecnologia finFET possono avere dimensioni molto piccole pur mantenendo buoni parametri elettrici. Tale caratteristica risulta essere molto importante quando si tratta di raggiungere un limite di rilevamento pari ad una singola molecola. Quando le molecole si legano alla superficie del dispositivo, la carica all'interno del canale viene redistribuita facendo sì che si verifichi una modulazione della corrente all'interno del dispositivo stesso. Il segnale derivante dalla presenza delle molecole dipende fortemente dalla natura della superficie alla quale si legano. Per questo motivo, due tipi diversi di amminosilani sono stati impiegati nel creare e caratterizzare due monostrati auto-assemblati alternativi. I due amminosilani sono: (3-amminopropil)trimetossisilano (APTMS) e (11-amminoundecil)trietossilano (AUTES). I due strati sono stati caratterizati in termini di angolo di contatto, spessore, carica superficiale e abilità di contatto. Dalle diverse tecniche di caratterizzazione della superficie sono stati ottenuti risultati coerenti e accurati, sulla base dei quali il migliore strato auto-assemblato è stato scelto per essere depositato sui transistors e poter proseguire alla loro caratterizzazione elettrica. In questa fase, l'ottima qualità dei dispositivi è stata dimostrata sula base di due parametri elettrici: la tensione di soglia dei transistors e la loro oscillazione sottosoglia. Questi parametri sono stati confrontati sia con valori ideali trovati in letteratura, sia con precedenti risultati sperimentali. I risultati derivanti dai biosensori funzionalizzati con amminosilani forniscono valori di oscillazione sottosoglia uguali ai biosensori che non sono stati sottoposti alla procedura di funzionalizzazione. Tale risultato dimostra che l'aggiunta di amminosilani non impedisce il buon funzionamento dei dispositivi. La

caratterizzazione elettrica termina con un protocollo in due fasi per la formazione di un legame tra 2μM 50A50T DNA oligonucleotidi e la superficie dei dispositivi, attraverso l'azione di un agente reticolante chiamato glutaraldeide. Gli esperimenti dimostrano un evidente cambiamento nella corrente del dispositivo dopo il legame della glutaraldeide con la superficie ricoperta di amminosilani. Tuttavia, la successiva aggiunta di DNA non risulta in una ulteriore modulazione della corrente. Esiti e possibili motivazioni di tali risultati sono analizzati e discussi al termine della parte relativa alla caratterizzazione elettrica. Infine, la tesi si conclude elencando i limiti presenti nello studio riportato ed esponendo possibili prospettive future su biosensori al silicio con tecnologia FETs.

Abbreviations

A	Adenine
AAM	All Area Modified
AFM	Atomic Force Microscope
APTMS	3-aminopropyltrimethoxysilane
ATR	Attenuated Total Reflectance
AUTES	11-aminoundecyltriethoxysilane
bioFET	Biological field-effect transistor
BOX	Buried Oxide
C	Cytosine
CA	Contact Angle
DIW	Deionized Water
DNA	Deoxyribonucleic acid
EDL	Electrical Double Layer
FET	Field-Effect Transistor
G	Guanine
GA	Glutaraldehyde
IEP	Isoelectric point
IPA	Isopropanol

MSE	Mean Squared Error
MOS	Metal Oxide Semiconductor
PBS	Phosphate-buffered saline
RU	Response Unit
SAM	Self-Assembled Monolayer
SOI	Silicon-On-Insulator
SDS	Sodium Dodecyl Sulphate
SMU	Source Measurement Unit
SPR	Surface Plasmon Resonance
SS	Subtreshold Swing
SSM	Selective Surface Modification
FGA	Forming Gas Annealing
FTIR	Fourier Transform InfraRed spectroscopy
T	Thymine
TIR	Total Internal Reflection
UV	Ultraviolet

Symbols

$[\ ]$	Concentration
Γ	Electrical conductivity of fluid
δ_D	Surface density
ϵ_0	Debye length
ϵ	Permittivity of free space
σ_c	Permittivity of the fluid
σ_e	Surface charge
Φ_M	Workfunction of metal
Φ_S	Workfunction of semiconductor
Ψ	Amplitude of light
Ψ_S	Semiconductor surface potential
Ψ_B	Bulk potential of semiconductor
Ψ_{DL}	EDL potential drop
μ	Charge carrier mobility
χ_s	Electron affinity of semiconductor
χ^{sol}	Surface dipole potential of the electrolyte
c_0	Bulk ion concentration

C_{OX}	Oxide capacitance per unit area
d_{st}	Stern Layer thickness
Δ	Phase of light
D	Diffusivity
E_0	Vacuum level
E_C	Conduction band energy
E_i	Intrinsic energy level
E_F	Fermi energy level
E_G	Energy bandgap
E_{REF}	Electrochemical potential of reference electrode
E_V	Valence band energy
η	Interfacial energy between phases
γ	Electrolyte viscosity
H_{ch}	FET channel height
$[H^+]_B$	Proton concentration at the bulk
$[H^+]_S$	Proton concentration at the oxide surface
I	Ionic strength
I_{DS}	Drain-source current

k_B	Boltzmann constant
K_a	Protonation constant
K_b	Dissociation constant
L_{ch}	FET channel length
m	Slope factor
n	Electron current density
n_i	Intrinsic electron current density
N_D	Donor dopant density
N_S	Surface density of oxide silanol groups
p	Hole carrier density
pH_B	pH in the bulk of the electrolyte
pH_S	pH at the oxide surface
q	Unit electric charge
Q_{IT}	Oxide surface charge density
Q_{OX}	Fixed oxide trap charge density
r	Reflectivity
T	Temperature
θ	Contact angle
V_0	Gate voltage at a specific I_{DS}

V_{DS}	Drain-source voltage
V_{FB}	Flat band voltage
V_{GS}	Gate-source voltage
V_M	Metal-semiconductor voltage
V_{th}	Threshold voltage
W_{ch}	FET channel width
ζ	Zeta potential
z	Valency of ions

Contents

Chapter 1

Introduction

Biomolecule sensing deals with the recognition of specific biological entities called target molecules within the sensor's environment. The presence of these target molecules is then transformed in a quantitative information, typically an electrical signal, which can be used to analyze the original sample. Biomolecule detection has become a hot topic in the scientific community since the discovery of well-known molecules like proteins, deoxyribonucleic acid (DNA) and virus in 19^{th} and 20^{th} centuries. Subsequently, a growing interest in biomolecule sensing started to arise especially after the discovery of a correlation between the presence of those biomolecules and early diseases' identifications. Often, an early medical diagnosis can make disease treatment much more efficient. Hence, the detection of a specific biological entity can play a crucial role in disease diagnostics. This explains why biosensing has become an attracting and expanding field in modern research.

This thesis contributes to the development of a new surface coating for biomolecule sensing by using some of the latest advances in silicon technology. Indeed, a lot of progress has been made in the last decades about biomolecule detection, but most of them have been implemented in ad-hoc solutions, unmanageable for mass production. In this thesis, we will focus our attention on bionsensors based on Field-Effect Transistors (FETs) at the nano-scale, using liquid-gate technology. Liquid-gate technology is the crucial part for biosensing in this work, because the liquid gate allows the target molecules to bind to the sensor's surface by means of a pressure-driven fluidic setup. Liquid-gated FETs are obtained by removing the metal gate of standard MOSFETs (metal-oxide-semiconductor FETs) exposing the FET's surface directly to the liquid environment.

The thesis is divided in three parts. First, a theoretical explanation of the working principle of the bioFET is presented. Then, a study of the best self-assembled monolayer (SAM) for silicon bioFETs has been investigated by means of surface characterization techniques. Eventually, the electrical characterization of the SAM coated bioFETs is shown. An outlook and possible future work on the development of functional coatings for bioFET sensors concludes the thesis.

1.1 Biosensors

Biosensors are devices which transform a biological event, like the binding of DNA, into a quantifiable (usually electric) signal. To fulfil this purpose, we can represent the biosensor as the sum of two main components: a bioreceptor, that means a biological entity able to recognize the desired molecule, and a transducer, a device which converts a physical quantity from one domain to another. In principle, any kind of molecule could be sensed, therefore the choice of the bioreceptor is not unique a priori. Depending on the type of target molecule, there will be an optimal type of receptor. A general description of the biosensing principle is expressed in **Figure 1.1**, which shows the biosensor structure together with some examples of bioreceptors and transducers.

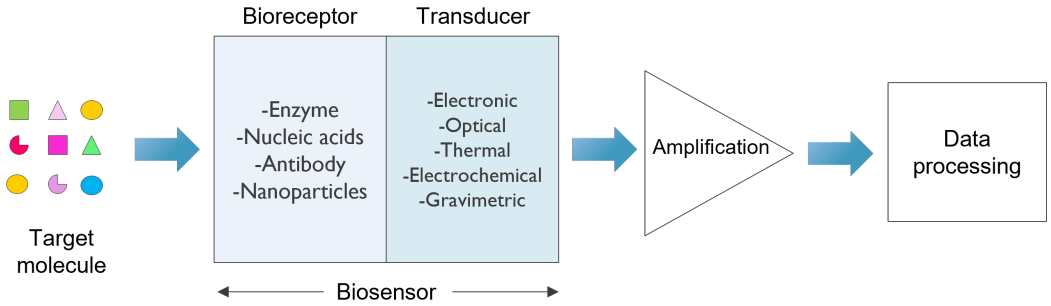

Figure 1.1: Structure of biosensors.

Bioreceptor and transducer are both fundamental blocks of a biosensor because they accomplish two different goals: the receptor defines the sensor's selectivity, while the transducer is responsible for the sensitivity of the sensor. Selectivity represents the ability of recognizing one specific type of analyte by isolating the desired molecule from all the rest. Sensitivity describes how large the signal becomes for a given concentration or amount of target molecules being detected. Together with the noise floor, the sensitivity determines the signal-to-noise ratio and consequently the detection limit of the sensor. Selectivity, sensitivity and noise are crucial characteristics of a biosensor and they are parameters that define the success of new biosensors launched on the market. In our work, we aim to increase the sensitivity of the bioFET sensor while maintaining a high specificity by means of the development and optimization of a new surface coating. First, we choose the target molecule and we design the best functional layer and binding protocol according to the specific biological entity (Chapter. 3). After the chemical characterization and optimization of the new surface coating, the functional layer is deposited on bioFETs to perform their electrical characterization. At this stage, the higher sensor sensitivity is achieved by using nano-scale FETs, which are known to result in higher single-molecule sensitivies [24]. The fabrication process of the finFETs used in this work is not part of this thesis.

1.1.1 Functionalization

Specificity over a target biomolecule is one of the most important parameter in a biosensor. Once you have designed a biosensor to detect a specific molecule, you expect it will be able to recognize the target no matter how many molecules are present simultaneously. A fair example is represented by the blood. Indeed, it is a common practise to collect a blood sample to discover if a patient has a certain disease or not. However, blood is a very complex fluid composed by many different types of cells. This means that the target molecule will not be the only one present in the sample. Hence, it is of relevant importance to be aware of the whole system when we embark on the design of a biosensor. Close attention must be paid to the environment in which the target molecule will be found, so as to avoid unwanted binding and untrue diagnosis.

In the world of biosensors we talk about sensor functionalization when we modify the sensor's surface to recognize a specific target molecule. The term functionalization is often substituted by immobilization of the target molecule, because only with a good immobilization process we can achieve a high quality sensor's selectivity. Therefore, the analyte's immobilization upon the transducer has to be fully understood. The immobilization mechanisms are divided in two main categories:

- surface binding: it involves chemical interactions between the analyte and the probe molecule;
- physical retention: it consists in a physical separation between the probe and the analyte.

Surface binding

In the binding mechanism the biologically active material is directly attached to the surface of the transducer. There are two different possibilities for the binding: adsorption and covalent binding.

1. Adsorption consists in the binding of probe molecules with the transducer's surface by means of not-permanent forces like Van Der Waals forces or hydrogen bonds. It is intrinsically a less invasive technique, whose pros and cons rely on the type of forces themselves. Since they are not proper chemical bonds, the binding is less effective, and it could lead to desorption of the active material. However, it will not denature the material itself, which is a crucial aspect in biosensing. The adsorption method is schematically shown in **Figure 1.2(a)**.
2. Covalent binding is represented in **Figure 1.2(b)**. It relies on the chemical binding of the probe molecule with both the surface of the transducer and the analyte. For this reason, the transducer's surface must be well-treated with reactive groups which allow for the first chemical bonding of the probe molecule. Then, the probe molecule has to be chosen properly, so as to own another functional group at the end that is able to bind also to the analyte. Intrinsically, the working principle of this mechanism represents a permanent binding. It has the largest lifetime and the

quickest response time, but there is the risk of denaturing the molecules, i.e in the case of proteins.

Physical retention

In the physical retention mechanism, a permeable layer is put on the surface of the transducer. Its feature is to be permeable to the analyte, but not to the biologically active material, so as the latter could stay permanently close to the surface. There are two different kind of methods: membrane confinement and membrane entrapment.

1. Membrane confinement involves the usage of a semipermeable membrane, which is capable of retaining only the target molecules. Semipermeable membranes have a pored structure, where the pores are big enough to allow the passage of the analyte and its products, but not the biological active material. Membrane confinement is depicted in **Figure1.2(c)**.

2. Membrane entrapment is shown in **Figure 1.2(d)**. It consists in the formation of a immobilization matrix, which is made of pores small enough to retain the biological active material, but big enough to allow the analyte crossing. In this technique, the ligand is not confined within a certain perimeter, but it is entrapped by a cross-linking agent.

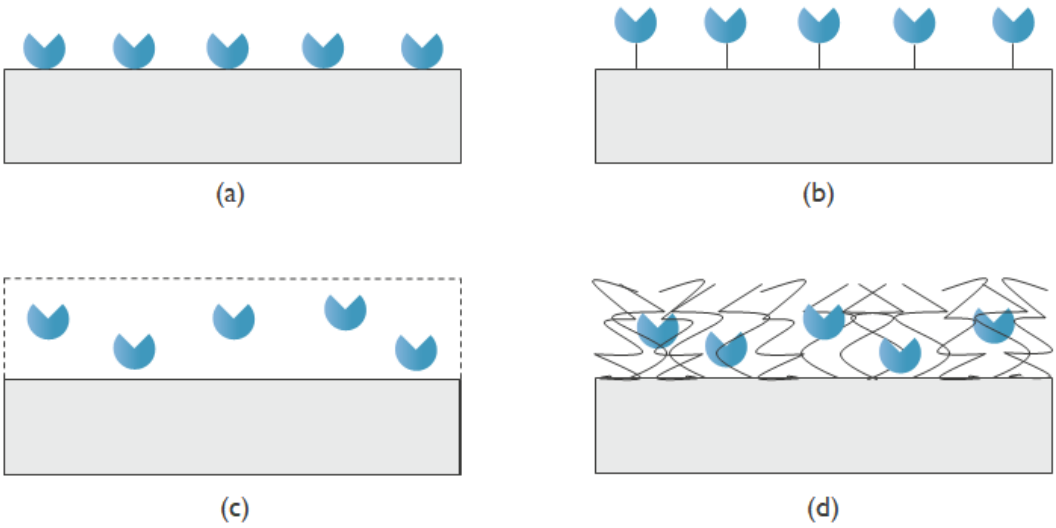

Figure 1.2: Immobilization techniques: (a) adsorption, (b) covalent binding, (c) membrane confinement, (d) matrix entrapment.

Self-assembled monolayer (SAM)

In this thesis work, the covalent binding mechanism is selected for the immobilization of biomolecules on the sensor's surface. The covalent attachment is achieved by means

of a deposited silane layer with functional end groups. The silane layer is deposited in the vapor phase and it self-assembles onto the surface forming a new coated surface. More specifically, the self-assembling process consists in the spontaneous organization of molecules with geometric repeated symmetry at the molecular level, after binding with the surface. In principle, a self-assembled monolayer (SAM) is composed by three different parts:

- a head group, which provides the chemical binding of the molecule to the sensor's surface. In our case, it is represented by a silane group, which binds to the silicon dioxide surface.
- a bulky group, which represents the largest amount of molecules forming the SAM. In the case of silane layer, it is identified by an apolar alkyl chain.
- terminal group, which is the last part of the SAM. In our case, it is represented by a functional amino end group to bind the target molecule.

The bulky group is the one forming the ordered layer by means of Van Der Waals forces. It is called self-assembled layer because it grows spontaneously under proper environmental conditions such as temperature and pressure. The described structure is represented in **Figure 1.3**.

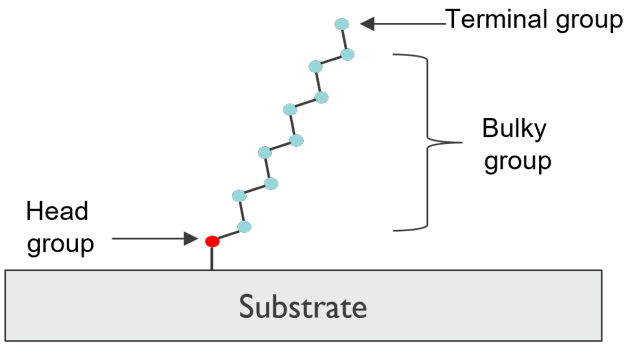

Figure 1.3: Zoom on an ideal self-assembled monolayer structure. In our ideal silane layer: the head group is represented by a silane group, the bulky group is identified by an apolar alkyl chain and the terminal group is the amino end group.

A self assembly monolayer is also a clear example of bottom-up approach, where complex structures are built starting from single molecules. The bottom-up approach is the opposite of the top-down approach, massively used in silicon technology. The idea of developing new nanodevices includes the usage of both approaches. Indeed, by using a bottom-up approach there is in general a larger variety within the self-assembled structures on the entire wafer's surface, while very good uniformity is reached with a top-down approach. On the other hand, with a bottom-up approach you can go further with smaller features, which are impossible to reach with standard top-down techniques. Also, self-assembled structures interact more naturally with the biological world. Therefore, the development of innovative and reliable bioFETs likely requires the exploitation and combination of

both the top-down and bottom-up approaches. For what concerns the devices used in this thesis work, they have been fabricated in the classical top-down approach based on photolithography. While, the bottom-up approach has been carried out only to coat the chip surface with the functional layer.

1.1.2 Transduction principle

Among the large variety of transducers, we focus on the ones involving the electrical detection. There are three mechanisms for electrical detection:

- amperometric transducers, which measure the resulting current of a redox reaction;
- potentiometric transducers, which measure a potential change at the electrodes;
- conductrometric transducers, which measure conductance or resistance changes in the ionic medium in between the electrodes.

In the following section, we will focus on the Field-Effect Transistor as a potentiometric transducer.

1.1.3 Metal-oxide-semiconductor field-effect transistor (MOSFET)

The potentiometric transducer is based on field-effect transistors, whose fundamental structure is the Metal-Oxide-Semiconductor (MOS) architecture. The MOS architecture is a three-layer structure where a potential well can be formed at the oxide's interfaces if a proper voltage is applied between the metal contact and the semiconductor layer. The creation of an energy barrier between the metal-oxide interface and the oxide-semiconductor is the consequence of the energy bands bending due to a charge distribution within the structure. According to the sign and absolute value of the applied voltage, together with the nature of the semiconductor layer, different behaviours arise. In the following, we will focus on MOS structures with n-type semiconductor layer to be coherent with the technology used in this work that exploits p-type FETs. An example of n-type MOS structure is depicted in **Figure 1.4**.

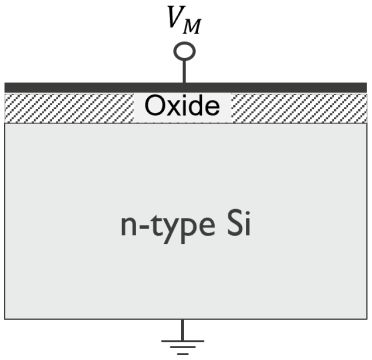

Figure 1.4: Metal-Oxide-Semiconductor (MOS) structure.

In an inversion mode p-type MOSFET the semiconductor layer is n-type. By considering silicon as selective material, in normal condition it has four electrons in the valence band. If a n-type doping process is carried out, it means that a little amount of Si atoms is replaced by atoms with five electrons in the outer shell, also called donor impurities. Examples of donor elements are Phosphorous (P), Arsenic (As) and Antimony (Sb). As a consequence of the doping, free electrons will form due to the lack of available locations in the valence bands of Si atoms. The result of a n-type doping is a Si layer with more free electrons, making electrons the majority carriers. At room temperature, the electron concentration is nearly equal to the donor concentration [6]. In other words, we can consider complete ionization at moderate (room) temperature. The energy band diagram of a n-type semiconductor has a Fermi level shifted towards the conduction band. This because the Fermi level represents the energy level of an electron with a probability of 50% to be occupied at any time (under thermodynamics equilibrium condition). So, if there are donor impurities that increase the number of electrons in the system, more electrons will be present in the conduction band with respect to the presence of holes in the valence band. As a consequence, the occupation probability of electrons in the conduction band will be greater than the one of holes in the valence band. The energy band diagram for an n-type doped semiconductor in equilibrium is depicted in **Figure 1.5**. The equilibrium condition is expressed by the constant Fermi level among the entire structure.

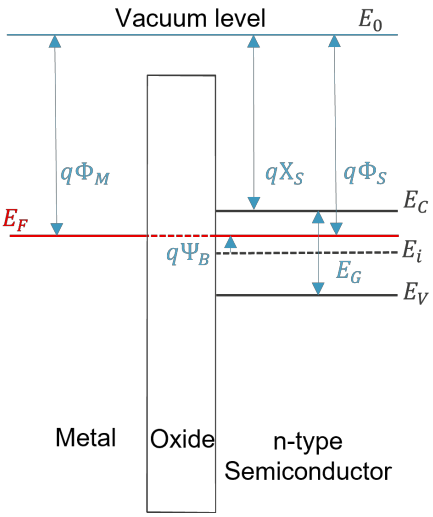

Figure 1.5: Energy band diagram of a MOS structure at equilibrium. $q\Phi_M$ and $q\Phi_S$ represent respectively the metal and semiconductor workfunctions. E_0 is the vacuum level and $q\chi_S$ is the electron affinity of the semiconductor. E_C and E_V are respectively the conduction and valence band of the semiconductor. Their difference is E_G, that is the energy gap. $q\Psi_B$ is the silicon bulk potential.

The energy band diagram depicted in figure 1.5 represents an ideal MOS structure with equal work functions of the semiconductor and metal. In reality, the metal and the semiconductor have different workfunctions ($q\Phi_M \not\equiv q\Phi_S$). Moreover, charges at the oxide's

interface must be taken into account. As a consequence, even without applied voltages, band bending in the semiconductor occurs. Therefore, in order to obtain flatband condition, a voltage must be applied to the metal contact. The metal voltage that results in the flat band condition is called the flat band voltage and its expression is the following:

$$V_{FB} = \Phi_M - \Phi_S - \frac{Q_{IT} + Q_{OX}}{C_{OX}} \tag{1.1}$$

where Q_{IT} stands for interface trapped charge and Q_{OX} represents the fixed oxide. C_{OX} is the oxide capacitance and it is proportional to the ratio of the dielectric constant and the thickness of the oxide.

The charge distribution within a p-type MOS structure depends on the type of applied voltage at the contacts. A simple analysis can be carried out if we consider the semiconductor contact to be grounded. In particular, two cases arise:

1. forward bias: $V_M > 0$. In this configuration, electrons in the semiconductor move towards the oxide layer, leading to an accumulation of electrons near the interface. If the applied voltage increases, more electrons will be accumulated. This behaviour does not change the intrinsic property of the Si layer, which remains a n-type semiconductor layer.

2. reverse bias: $V_M < 0$. By decreasing the applied voltage a new situation occurs. Electrons in the semiconductor move towards the bulk, leading to accumulation of holes near the oxide interface. The Fermi level of the metal rises up and the energy bands in the semiconductor starts bending upwards. If the absolute value of the negative voltage becomes higher, at a certain point the intrinsic energy level of the semiconductor overcomes the Fermi level. As a consequence, more holes are present near the oxide surface, and the Si layer behaves like a p-type semiconductor. This phenomenon is called charge inversion and an inversion layer is formed.

The working principle is graphically represented in **Figure 1.6**, where all the previous steps are depicted.

To form a MOSFET structure, two other terminals called drain and source are added to the configuration. They are connected to two highly-doped p-type regions in the Si layer. An example of this structure is represented in **Figure 1.7**.
The concept of MOSFETs consists in the generation of a current between the two highly-doped p-type regions in the Si layer, when applying a voltage to the metal contact also called gate terminal. This is possible thanks to the holes' inversion layer formed near the oxide's interface, together with the applied voltage between source and drain which which results in a hole current from source to drain. Applying a potential to the gate creates a field across the oxide and the semiconductor changing the semiconductor carrier concentration and consequently changing the conductance of the semiconducting channel. Through the modulation of the applied voltage, the field strength changes, and so does the hole concentration and consequently the current.

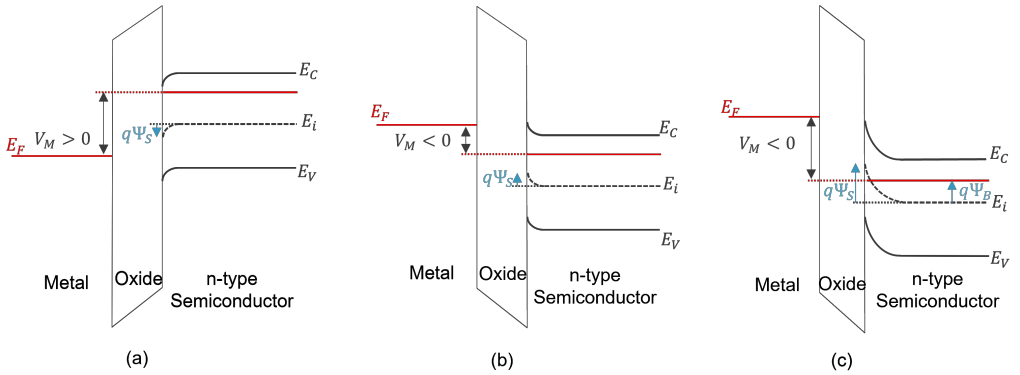

Figure 1.6: Energy bands in a MOS structure: (a) accumulation, (b) depletion and (c) inversion. V_M is the applied voltage at the metal contact. $q\Psi_S$ is the energy band bending at the semiconductor's surface, also called surface potential. An inversion layer arises for a surface potential equal to approximately twice the bulk potential.

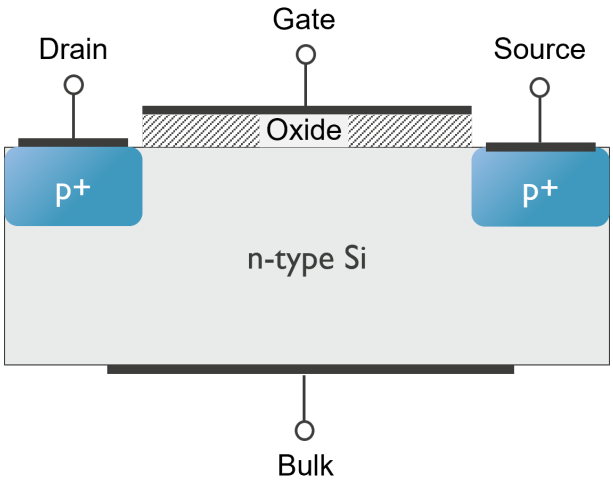

Figure 1.7: p-type MOSFET structure.

The gate voltage needed to reach the on-state is called threshold voltage (V_{th}). The threshold voltage is a key parameter for MOSFETs because it distinguishes between different working regions of the transistor. Its expression is the following:

$$V_{th} = V_{FB} + 2\Psi_B - \frac{\sqrt{4\epsilon_{Si} q N_D |\Psi_B|}}{C_{OX}} \tag{1.2}$$

where V_{FB} is the flat band voltage, that is the gate voltage for which the surface potential in the semiconductor is zero, as previously shown in **Figure 1.5**. ϵ_S is the absolute

permittivity of silicon, while the bulk potential ($q\Psi_B$) of the semiconductor can be investigated once the amount of donors (N_D) is known. Its expression is equal to:

$$\Psi_B = -\frac{k_B T}{q} \ln\left(\frac{N_D}{n_i}\right) \tag{1.3}$$

where k_B is the Boltzmann constant, T refers to the operating temperature, q is the Coulomb charge and n_i is the intrinsic carrier density in silicon.

In a p-type MOSFET which works in the inversion region, threshold voltages typically have a negative value such that they are non-conducting in absence of a gate voltage. For gate voltages more negative than the threshold voltage, the FET is turned on. As stated before, it means that a high-density inversion layer is formed between drain and source regions, near the oxide layer. Usually, the inversion layer does not form homogeneously in the semiconductor. In particular, when a negative voltage is applied from drain to source, the inversion layer starts forming near to the source region first. Thus, typically the gate voltage is expressed as the voltage from gate to source terminal (V_{GS}). The value of this voltage with respect to the threshold defines the operating condition of the MOSFET. By focusing on the well-known threshold based model [31], also called piecewise model, two different working regions can be identified. In the case of p-type FETs, the subthreshold region is defined as the working region where the (negative) gate-to-source voltage is approaching the (negative) threshold voltage, but where a conductive inversion layer is not completely formed yet. In the subthreshold condition (V_{GS}-$V_{th} > 0$), the drain current I_{DS} follows an exponential behavior that can be described by the following expression, when both the body-effect and the drain-induced barrier lowering (DIBL) effect are neglected [7]:

$$I_{DS,subth} = \frac{\mu_p W_{ch} C_{ox}}{L_{ch}} \left(\frac{k_B T}{q}\right)^2 (m-1)(1 - e^{\frac{qV_{DS}}{k_B T}}) \cdot e^{\frac{-q(V_{GS}-V_{th})}{m k_B T}} \tag{1.4}$$

The new parameters appearing in **Equation 1.4** refer to the transistor's dimensions and performances. μ_p is the charge carrier mobility in the channel (p-type), W_{ch} is the channel width, L_{ch} is the channel length and m is called slope factor. The subthreshold swing (SS) indicates how efficient a FET can be turned on and off. The smaller the SS value, the closer the FET approximates an ideal switch. The SS is related to the slope factor itself by the following formula:

$$SS = \frac{dV_{GS}}{d \log I_{DS}} \sim 2.3m \frac{k_B T}{q} \tag{1.5}$$

Ideally, the slope factor is unitary and for temperature equal to 300K (room temperature) the subthreshold swing reaches its minimum value (SS $\sim 60mV/dec$). Using the threshold voltage and the subthreshold swing parameters, the subthreshold drain current formula can be rewritten as follows:

$$I_{DS,subth} = I_0 \cdot e^{\frac{2.3(V_{th}-V_{GS})}{SS}} \tag{1.6}$$

where the variable I_0 contains all the quantities independent of the gate-to-source voltage, already listed before. **Equation 1.6** shows how the two fundamental parameters of the FETs (V_{th} snd SS) determine the drain current.

In a p-type MOSFET, above the threshold (V_{GS}-$V_{th} < 0$) an inversion layer consisting of holes is formed near the oxide surface. The inversion layer forms a conductive channel is formed between the two highly doped p regions of the source and drain. In this regime, the current increases linearly with the gate-to-source voltage. The drain current expression in this linear regime is represented by the following expression:

$$I_{DS,lin} = \frac{\mu_p W_{ch} C_{ox}}{L_{ch}} \left[(V_{GS} - V_{th}) V_{DS} - \left(\frac{V_{DS}}{2} \right)^2 \right] \tag{1.7}$$

By combining the expressions of the drain current below and above the threshold, the FET current can be approximated for the entire gate voltage range. In Chapter 4, the $I_{DS} - V_{GS}$ characteristics of the FET sensors are measured both below and above the threshold. Hence, a comparison between the measured and modeled drain current can be obtained.

1.1.4 Ion-sensitive field-effect transistor (ISFET)

There is a structural difference between MOSFETs and ISFETs. In an ISFET, the metal gate is removed such that a cavity is formed. Liquid-gating is realized by filling the cavity with an electrolyte solution and contacting the electrolyte with a reference electrode. By definition, an electrolyte solution is a solution with charged particles, i.e ions, that make the fluid electrically conductive. The ion sensitivity of ISFETs originates from the interaction between the ions in the electrolyte and the gate oxide. More specifically, the interaction between the ions in the electrolyte and the oxide surface results in changes of the oxide surface charge. Consequently, the change in oxide surface charge modifies the drain current as well. This variation in drain current due to the electrolyte-oxide interaction results in an additional term in the threshold voltage. The formula of the threshold voltage valid for ISFETs is the following [20]:

$$V_{th} = E_{REF} - \chi^{sol} - \Psi_{DL} - \frac{\Phi_S}{q} + 2\Psi_B - \frac{Q_{OX} + \sqrt{4\epsilon_{Si} q N_D |\Psi_B|}}{C_{OX}} \tag{1.8}$$

where E_{REF} is the constant potential of the reference electrode and χ^{sol} is the surface dipole potential only related to the type of electrolyte solution. Ψ_{DL} is the interfacial potential between the oxide and the electrolyte solution, that is equivalent to the potential drop across the Electrical Double Layer (EDL) formed at the oxide's surface. For what concerns the other parameters, they remain unchanged with respect to the expression of the MOSFET threshold voltage. Among the listed parameters, the potential drop across the EDL is the major responsible for the threshold voltage shift arising due to the ion interaction with the FET surface. Hence, the mechanism involving the creation of an

electrical double layer above the device's surface has to be fully understood.

In general, when a dielectric material is immersed in an electrolyte solution, a surface charge arises. The most important ion that impacts the oxide surface charge is the hydronium ion (H_3O^+) typically represented by (H^+). The (H^+) concentration is directly linked to the pH (pH=-log[(H^+)]) giving oxide surfaces their typical pH-dependent surface charge. More specifically, the surface charge originates from the association and dissociation reaction between the (H^+) ions in the electrolyte and the silanol groups on the oxide surface (-OH). Three situations can occur depending on both the concentration of hydronium ions at the oxide surface and the pH of the electrolyte solution. Silanols groups ($-OH$) can be either deprotonated to form negatively charged $-OH^-$ groups, protonated to form positively charged $-OH_2^+$ groups or unprotonated to remain neutral $-OH$ groups. The dissociation reactions of silanol groups are the following [32]:

$$SiOH_2^+ \rightleftharpoons SiOH + H^+ \qquad with\ dissociation\ constant : K_a \tag{1.9}$$

$$SiOH \rightleftharpoons SiOH^- + H^+ \qquad with\ dissociation\ constant : K_b \tag{1.10}$$

The pH and the dissociation constants of the chemical dissociation reactions determine which situation dominates. The following expressions hold for the dissociation reactions:

$$K_a = \frac{\Gamma_{SiOH} \cdot [H^+]_S}{\Gamma_{SiOH_2^+}} \tag{1.11}$$

$$K_b = \frac{\Gamma_{SiO^-} \cdot [H^+]_S}{\Gamma_{SiOH}} \tag{1.12}$$

where for simplicity the proton concentration at the surface $[H^+]_S$ is equal to the hydronium concentration $[H_3O^+]$ cited before. Γ represents the surface density of the different groups present at the oxide surface. For example, $\Gamma_{SiOH_2^+}$ is the amount of protonated silanols groups, while Γ_{SiO^-} is the surface density of the deprotonated silanols groups. Their values can be extrapolated by reversing **Equation 1.11** and **Equation 1.12**, and by knowing the total density of silanols groups at the surface $N_S = (\Gamma_{SiOH_2^+} + \Gamma_{SiOH} + \Gamma_{SiO^-})$. Typically, the equilibrium dissociation constants are described by their logarithm, pK=-log(K). The values of pKa and pKb for silicon dioxide are quantities that can be found on the internet. While, the surface proton concentration is linked to the bulk proton concentration by Boltzmann statistics: [3]:

$$[H^+]_S = [H^+]_B \cdot e^{\frac{-q\Psi_{DL}}{k_B T}} \tag{1.13}$$

The relationship between the solution's bulk pH and the bulk proton concentration is given by:

$$[H^+]_B = 10^{(-pH_B)} \tag{1.14}$$

The net charge density of the surface is found by subtracting the positively charged (protonated) from the negatively charged (deprotonated) surface groups. This leads to the following expression: [3]:

$$Q_{int} = qN_S\left(\frac{[H^+]_S^2 - K_aK_b}{[H^+]_S^2 + K_a[H^+]_S + K_bK_a}\right) \tag{1.15}$$

In the case of silicon dioxide surfaces, the total density of available sites for silanol groups (N_S) is about $4.5 \cdot 10^{18} molecules/m^{-2}$ [32], while the values of pKa and pKb are respectively -1.9 and 7.5 [32]. Based on these parameters, and considering the expression of the net oxide surface charge per unit area (**Equation 1.15**), silicon dioxide surfaces become negatively charged for pH values larger than 4. For lower pH values, the oxide surface becomes almost neutral. More specifically, the pH value for which the charged surface becomes uncharged is also called Point of Zero Charge (PZC). In the case of silicon dioxide surfaces, it is equal to pH 2-3.

Next to the pH-dependent surface charge density, another effect has to be considered in the working principle of ISFETs. This effect is the charge screening effect which originates from the redistribution of electrolyte ions near the charged oxide surface. The region where the redistribution of electrolyte ions occurs is called the Electrical Double Layer (EDL). Since there is a charge imbalance in the electrical double layer, an electric field arises and consequently a potential drop occurs. This quantity can be related to the charge stored in the electrical double layer by combining the ion distribution described by Boltzmann statistics [32] and Poisson's equation. Then, by considering the oxide surface charge to be equal (in magnitude) but opposite to the charge stored in the electrical double layer, another expression for the pH-dependent surface charge density can be obtained:

$$Q_{DL} = -Q_{int} = -\sqrt{8\epsilon k_B T c_0}\sinh\left(\frac{zq\Psi_{DL}}{k_B T}\right) \tag{1.16}$$

where c_0 represents the bulk electrolyte ion concentration and z represents the valency of the ion species in the electrolyte solution.

The formation of the electrical double layer can be described by the Gouy-Chapman-Stern model [32]. A simple schematic representation of the EDL is represented in **Figure 1.8**.
The model divides the EDL in two layers. The layer closest to the surface is free of fixed ions that make it a molecule-thick layer. It is called the Stern layer. The second layer is the diffuse layer in which mobile ions are present. In this layer electrolyte charge screening occurs due to the redistribution of mobile electrolyte ions. The potential drop across the diffuse layer is described by a near-exponential decay. This near-exponential trend follows from the Poisson equation and Boltzmann statistics. The decay length of

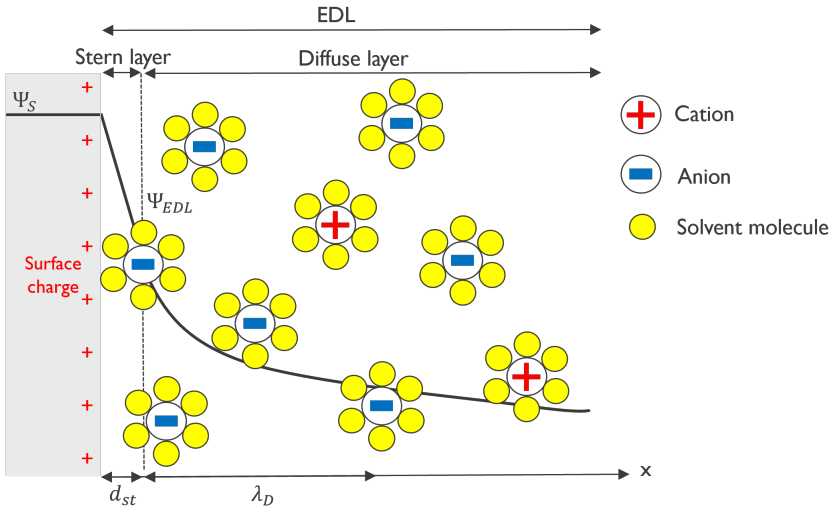

Figure 1.8: Structure of the electrical double layer (EDL).

the exponential behavior is better known as the Debye length:

$$\lambda_D = \sqrt{\frac{\epsilon k_B T}{2q^2 I}} \tag{1.17}$$

with ϵ equals to the electrolyte's permittivity and I representing the ionic strength of the electrolyte solution. The result of this analysis shows how the Debye length can be affected by adjusting the ionic strength of the electrolyte solution. More specifically, the higher is the ionic strength, the smaller the Debye length becomes. As a consequence, the electrolyte charge screening strength increases and the double layer potential drop decreases, with the result that the ion-sensitive device becomes less sensitive. In other words, the ISFET's pH sensitivity increases for larger Debye lengths.

1.2 BioFET sensors

Starting from the definition of ISFETs, a bioFET sensor is obtained by simply functionalizing the gate oxide surface to interact with specific types of molecules in the electrolyte solution. More specifically, the presence of a functional layer on the FET surface which defines the sensor specificity towards a particular type of biomolecule is the biggest difference between ISFETs and bioFETs. A schematic example of a p-type bioFET sensor is represented in **Figure 1.9**.

The functional layer added to the ISFET structure has to be specifically designed in order to allow the binding of target molecules and prevent the binding of other molecules. For this reason, the target molecule must be chosen first. Then, the type of immobilization technique of the target molecule with the FET surface has to be selected among the ones already listed in Sec. 1.1.1. Whatever is the selected immobilization technique, the

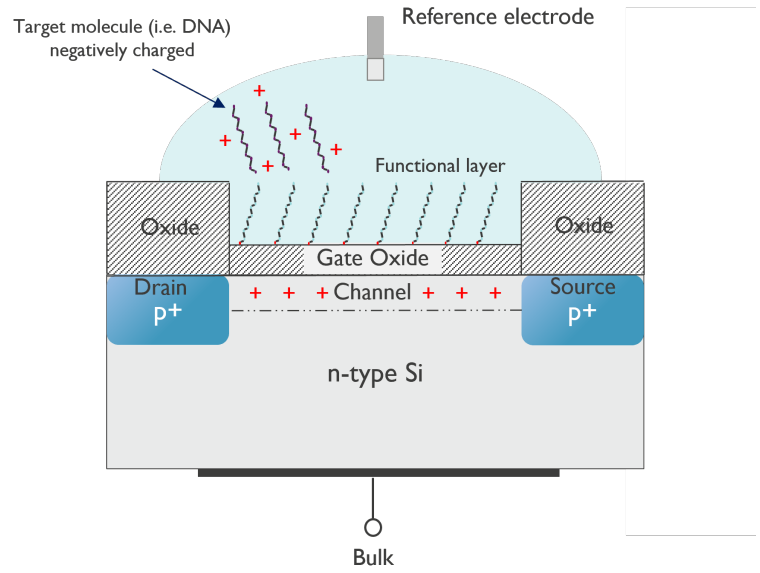

Figure 1.9: Schematic structure of a p-type bioFET sensor. In the example, negatively charged target molecules induce the screening of positive ions in the electrolyte solution near the functional layer, together with positive charge in the FET's conductive channel.

target molecule will always bind to the functional layer, and not to the oxide surface. Therefore, the target molecules bind at a certain distance from the surface such that the biomolecule signal is intrinsically different from the ISFET signal. In the specific case of p-type bioFET sensors and negatively charged target molecules, the biological event results in an increase of holes in the semiconductor channel. Which increases the current for p-type MOSFETs or makes the threshold voltage more positive. Both effects are schematized in **Figure 1.10**.

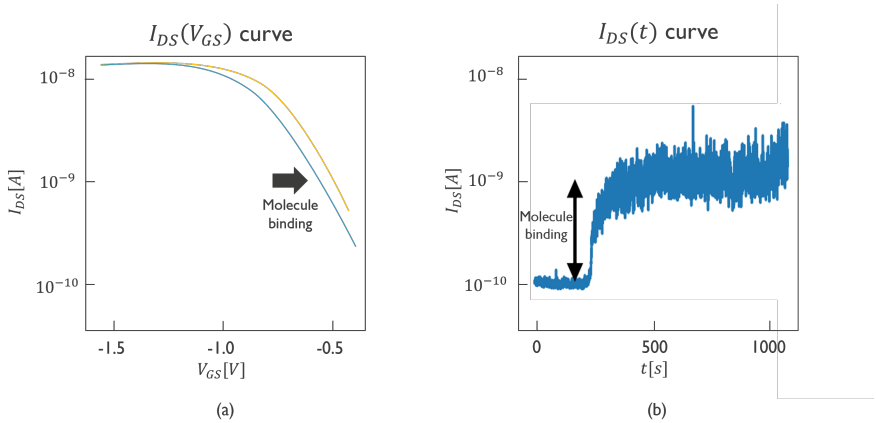

Figure 1.10: Biomolecule signal in a p-type bioFET. (a) positive threshold voltage shift, (b) drain current increase.

In the previous section, the explanation why the nature of the bioFET's surface is important has been described. However, two important factors that can modify the surface properties are the non linear screening and the pH interference effect. More specifically, the nonlinear screening locally enhances charge screening and it is triggered by highly charged surfaces. It derives from the local high electrolyte screening strength explained in Sec. 1.1.4. To limit this effect, we would like a surface which is less charged. Secondly, the pH sensitivity of the surface induces further charge screening when the target molecule binds to the FET surface. These charges are called counter charges and they derive by the local change in pH caused by the charge of the target molecule itself [25]. To avoid this effect, we would like a less pH-sensitive surface, which interferes less with biosensing.

To tackle both these issues, a less charged and pH-dependent surface is the goal to achieve to optimize the surface coating and to enhance the bioFET signal. Therefore, the key question of this research is: "Is it possible to develop a surface coating with low surface charge and low pH sensitivity while still maintaining a functional bioFET sensor?" The expected boost in bioFET sensitivity due to surface engineering could be a key factor to enable single-molecule detection with silicon-based bioFETs. Consequently, this realization could open doors for breakthroughs in high-end applications like sequencing and DNA storage.

Chapter 2

Methodology

The following chapter lists and describes the techniques used throughout this thesis work with the aim to allow whoever interested in replicating the experiments. First, the materials and the process steps for the coating procedure are depicted. Then, all the different characterization techniques used to extract useful parameters about the SAM are explained in detail. Consequently, the FET fabrication and the molecule functionalization procedure are described. Eventually, the setup and the protocols for the electrical characterization of the functionalized bioFETs close this chapter.

2.1 Silane layers: materials and preparation

Immobilization of biological elements is a crucial aspect for the implementation of biosensors. For this reason, a lot of effort has been made in this thesis work to obtain the best sensor's specificity. In order to fulfill this goal, first a deep study about surface engineering has been carried out on bare oxide samples. It means that deposition processes have been performed on thermal oxide Si substrates in order to characterize the SAM on a flat surface first. Later, after coating optimization, the same deposition process has been replicated on bioFETs in order to proceed with the electrical characterization. Therefore, all the following surface analytical techniques refer to Si substrates, where the only treatment performed before the chemistry deposition is the thermal oxidation (100 nm thickness).

The first thing to do when embarking in the design of a new SAM is to identify the best material for our purposes. Previous works on the same topic have been carried out by choosing a 11-Azidoundecyltrimethoxysilane ($C_{11}N_3$-silane) self-assembled monolayer [24]. The terminal group (N_3) of such SAM provides negatively surface charge on top of the structure. As a consequence, in the case of DNA as target molecule, the resulting layer seems to be not ideal to favorite the binding between the azide group of the SAM and the negatively charged oligonucleotides. The reason is the impact of the non-linear screening effect induced by the EDL on the FET sensitivity [19]. More in detail, Gupta et al show the correlation between surface charge and bioFET signal, and they demonstrate that tuning the surface charge is a solution in order to boost the

FET signal. In particular, a neutral or slightly positive surface charge results is the best option to maximize the FET sensitivity [19]. For this reason, in this thesis work we focus on aminoalkylsilane layers because of beneficial characteristics such as their bifunctional nature and low cost [1]. Specifically, we consider two different kind of aminosilane coatings. First, a well-known silane coupling agent called 3-Aminopropyltrimethoxysilane (APTMS) is considered, then an aminoalkylsilane with a longer carbon chain called 11-aminoundecyltriethoxysilane (AUTES) is taken into account. The one resulting as the best in terms of performances will be selected for the bioFETs functionalization.

The aminoalkylsilane self-assembled monolayer can be prepared both in liquid or vapor phase conditions [10]. However, in this thesis work only the latter approach is described because it has been demonstrated to be the more reliable and optimal one [11]. The first step to carry out before the coating process is the samples' preparation. The protocol used in this thesis involves a wet chemistry procedure, also called solvent cleaning. First, the samples are rinsed abundantly with acetone and isopropanol (IPA) to remove organic impurities that may be present on the surface after the samples' manipulation. High attention must be paid to rinse completely the samples' surfaces. For instance, by cleaning also the surface's part remained cover by the tweezers used to grab the sample itself. For this reason, usually the previous steps are performed more than once to be sure that all the sample's surface has been properly cleaned. After the rinsing procedure, the samples are well-dried by means of Nitrogen gun (N2). Thereafter, a 15min UV-O3 cleaning procedure is performed as further sureness of organic-contamination removal. This last step is performed immediately before loading the samples in the proper oven, so as to obtain a clean surface where the chemistry can easily bind to the silanol (Si-OH) groups.

After the surface cleaning, the samples are ready to be coated. The vapor-phase silanization process is the same for both type of chemistry used in this work, a part from the different parameters involved in the process: temperature, pressure, time and amount of chemistry. For APTMS coating, the deposition procedure consists in a 2h process in which the samples are placed on a ceramic plate inside a glass desiccator, which is loaded in an oven (Heratherm, Thermo Scientific) heated up to reach 120°. On the bottom of the desiccator, an aluminum cup is inserted exactly at the center of the ceramic plate, where a bigger hole is present. Inside the cup, 200μL of chemistry is loaded. That hole, together with other small holes among all the ceramic plate surface, allow to distribute homogeneously the chemistry at the vapor-phase inside the chamber. Before starting with the two hours deposition time, the pressure has to be adjusted to reach 25mbar. This is done by using a vacuum pump (Buchi V-300) connected to a stopcock at the top side of the desiccator through a silicone tube. For AUTES coating, the protocol includes the same pressure, but higher temperature (up to 140°) and higher deposition time (4h). A lower amount of chemistry is needed within this time frame (100μL is enough). Higher temperature and higher deposition time are required because of the longer chain of carbon present in AUTES molecule, which increases the SAM's building up process time. It is relevant to state that this last protocol could be further optimized, for example by

modifying the pressure parameter, which has never been changed during this work.

2.2 Chemical characterization

After the surface's functionalization with the chosen chemistry, it is fundamental to check the result of the vapor phase deposition. Among many types of existing characterization techniques, in this thesis work the following measurements have been carried out after each deposition process:

- Contact angle
- Ellipsometry
- Surface Potential
- Fourier Transform InfraRed spectroscopy
- Surface Plasmon Resonances.

In the following, a brief description of each characterization technique is given, together with the methodology used during the measurements.

2.2.1 Contact Angle

Contact Angle (CA) measurements study the wettability of the coated surface by using the *sessile drop method*. It consists in applying a drop of distilled water (or other test liquid) over the sample surface and measuring the contact angle formed at the three-phase interface (solid−liquid−gas) [4]. The liquid we use is Deionized Water (DIW), and each droplet has 1 μl volume. The measurement is performed immediately after the vapor phase deposition procedure, at room temperature. The software used for CA measurements is called *SCA20*. It automatically computes the contact angle by means of the Young's equation [5]:

$$\gamma_{lv} cos\theta = \gamma_{sv} - \gamma_{sl} \tag{2.1}$$

where γ_{lv}, γ_{sv} and γ_{sl} represent the interfacial energies between the three phases (liquid, solid and vapor) and θ is the contact angle.

Contact Angle measurements are performed over five samples, which are coated with the same chemistry, but they differ in localization within the desiccator. Therefore, there will be CA results from samples in the top, left, bottom, right and central part of the desiccator. This procedure is important to have an idea of the spatial homogeneity of the vapor phase deposition within the desiccator. Moreover, for each sample we run five times the same measurement by only changing the contact point of the droplet within the sample's surface. This strategy is useful to study a minimum of statistics on our results and to check that the chemistry has been deposited homogeneously on the total sample's surface. In theory, we would like the results to be independent from both the

spatial location of the samples in the desiccator and the measurement point within the sample itself. In practice, we will see that there is always a certain deviation among the measurements.

2.2.2 Ellipsometry

Ellipsometry is an optical characterization technique for the determination of sample's parameters like thickness and optical constants of thin layers. The optical principle is the Fresnel law, where linearly polarized light hits the sample's surface first. Then, it is partially transmitted and finally reflected through the sample itself. In RC2 Ellipsometer tool (by J.A Woolam) the collected light is the reflected one, whose final polarization becomes elliptical. Indeed, the name of this technique itself expresses the type of polarization that light assumes after the sample reflection. What is acquired by the tool is the change in the polarization state, which is defined by means of amplitude (Ψ) and phase (Δ) values of the reflected light. The following formula defines mathematically these two parameters [14]:

$$tan(\Psi) \cdot e^{(i\Delta)} = \rho = \frac{r_p}{r_s} \tag{2.2}$$

ρ is a complex number and it represents the ratio between the p-polarized light reflectivity and the s-polarized light one. Ψ and Δ are the measured values from which samples' parameters can be extracted by means of a model-base approach. The software related to RC2 Ellipsometer (by J.A Woolam) is called *CompleteEASE*. It represents the tool where the model of the layered structure can be designed. Also, it is used to restore the sample's thickness after the measurement.

The correct model for the samples coated with the chosen chemistry is a three-layers model composed by a thick silicon substrate, a thin silicon dioxide layer and the upper SAM. During the measurements, light will be reflected at each interface between different type of surfaces. For the determination of the SAM thickness, the only interface we are interested in is the one between SAM and SiO2 layer. For this reason, when performing ellipsometry measurements on coated samples, the thickness of the underline SiO2 layer has to be known in advance. It is necessary to get one unknown parameter only, which will be uniquely related to the resulting amplitude and phase values. Therefore, a bare oxide silicon sample is always necessary to perform thickness measurements on the developed functional layer. This sample is also called *blanket* and it will act as a reference for our measurements.

Before performing ellipsometry measurements, some settings must be adjusted. Some of them are the angles formed by the beam and the plane of incidence, and the sample's points where the light will be focused to. In our protocol, three different angles are investigated, they are 65°, 70° and 75°. Furthermore, we always use a nine-points measurement approach forming a snake-path on the sample's surface. It is used to have also an idea about the sample's uniformity.

2.2.3 Zeta Potential

Every time a dielectric layer gets in contact with an electrolyte solution, surface charges form at the interface between the layer and the fluid. Thanks to Coulomb forces, ions of the electrolyte solution start screening the charges at the oxide surface. As a result, an Electrical Double Layer (EDL) forms. Consequently, the surface charge causes the formation of a potential drop within the electrolyte solution, close to the surface's boundaries. First, this potential is described by a linear trend. Then, as the distance from the surface increases, it is followed by a decreasing exponential behavior. More specifically, the linear trend is found in correspondence of the so-called Stern layer, characterized by fixed charges. While, the exponential drop of the potential arises within the so-called diffuse layer, which is made of mobile charges. The relevant value of the distribution is the surface potential value at the boundary between the two layers, which is called zeta potential. The theory about the surface potential has been discussed in Sec. 1.1.4, where an analytical description is reported. Here, we focus on the methodology of the surface potential measurements performed in this thesis work.

Surface potential measurements are carried out using SurPASS 3 tool (by Anton Paar). For this kind of measurements, two samples are required at the same time. Each sample is fixed to a support and the coated surfaces face each others, so as to form a micro-metric channel where the fluid can pass through. Once the measurement starts, the electrolyte solution passes all along the channel, giving rise to the EDL formation. Then, the software analyzes the voltage by means of the following equation [33]:

$$\zeta = \frac{dI_{str}}{d\delta p}\frac{\eta}{\epsilon\epsilon_0}\frac{L}{A} \tag{2.3}$$

where the first ratio represents the slope of the streaming current with respect to the differential pressure, η is the electrolyte viscosity, ϵ is the dielectric coefficient of the electrolyte, and L (length) and A (cross-section) are the geometrical parameters of the channel.

As working method, we repeat the measurement for different pH values, implementing a so called *pH Scan*. It consists in determining the zeta potential for different pH values. For our purposes, we would be interested just in the zeta potential at neutral pH, since in principle biological samples are intrinsically found in a pH neutral environment. However, in order to accomplish a more general analysis on the new SAM, we perform the measurements for a wide spectrum of pH values. In particular, we analyze from pH 3 to pH 11. The electrolyte solution we use is a 200µL DIW-based solution made acidic or basic respectively thanks to 0.05M HCl solution or 0.05M NaOH solution. The ionic strenght of the electrolyte solution is kept fixed at 10^{-3}M by means of the strategy explained hereinafter. We divide the pH Scan measurement in two. First, we perform a pH Scan from 3 to 7, making the electrolyte solution less acidic time by time. Then, we take a fresh solution and we perform a pH Scan from 11 to 7, making the electrolyte solution less basic step by step. In this way, we avoid the ionic strength to double within a single ramp, and we maintain it constant to 10^{-3}M. Before starting, the pH probe has to be

calibrated. The calibration is performed by inserting the pH probe in three solutions characterized by different pH values (pH=4,7,10).

Before running a zeta potential measurement, it is necessary to check that the gap size between the two samples is within 100 and 120 um. This range is the one recommended by the manufacturer in the guide of SurPASS 3 software. If the gap is not within this range, we can easily adjust it by rotating a knob in front of the tool and repeating the rinse procedure. In any case, a minimum rinsing of two times is necessary to make the machine ready to work properly. Once the gap is fixed, we can start the pH scan measurement. Typically, zeta potential measurements are performed more times for each pH value to obtain statistical relevant results. In our case, they are performed four times. Then, the mean value and the standard deviation for each pH value are calculated. These parameters are the two variables used in the *Python* simulation to graphically represent the experimental results.

2.2.4 FTIR

Fourier Transform InfraRed spectroscopy is a characterization technique useful for the elemental surface analysis of a material. It takes advantage of an infrared light source, which is absorbed in different amounts by the chemical species present on the sample. Each type of covalent bond induces a different kind of vibration when IR light is absorbed. Therefore, by collecting the absorbance of light as a function of frequency we obtain a full spectrum of the chemical composition of the analyte.

To accomplish this goal, we use an attenuated total reflectance Fourier transform infrared spectroscopy (ATR-FTIR). This means that the incoming light striking the sample is completely absorbed or reflected, without being transmitted through the sample itself. The ATR-FTIR tool exploited in Imec is a Thermo Scientific Nicolet 6700 spectrometer (by Thermo Fisher Scientific Inc.) with a VariGATR grazing angle accessory (by Harrick Scientific Products Inc.). The specifics for our measurements include a grazing angle of 65°, a Ge crystal as reflected element and IR p-polarized light. Liquid nitrogen (N_2) is needed to cool down the IR detector (made of mercury cadmium telluride), and it takes about thirty minutes to be ready to use. The spectral resolution is 4 cm^{-1} and 60 scans are performed for each measurement. 60 scans seems a good compromise between resolution and execution time. These specifications have been indicated in the *OMNIC* software, that is the tool where the measurements are launched.

First, the measurement is always performed on the blanket because it acts as a reference to check whether the chemistry has been correctly deposited or not. In principle, the NH2 peaks relative to the end part of the SAM should not be present on the blanket's spectrum. Differently, a clear peak in correspondence of the NH2 stretching bond wavelength is expected to occur in the coated samples' spectra. In order to properly compare the results, a post processing analysis is performed by using the *EssentialFTIR* software. The spectra are improved by using a five-points manual baseline correction plus a normalization to the Ge peak around 900 cm^{-1} that is always present in the measurements.

Indeed, as already mentioned a germanium crystal is used here as reflected element. So, the Ge peak is related to the longitudinal optical (LO) asymmetrical stretching of germanium oxide present on the Ge crystal. Which is caused by the partial reflection and enhancement of the evanescent wave at the Si substrate [16]. The analysis of the complete spectra has been carried out thanks to the help a proper manual [18].

2.2.5 SPR

Until now, we have analyzed the surface's properties of the functionalized dummy samples without involving DNA. However, DNA is the target molecule we would like to detect with our bioFETs. Therefore, it is important to test the binding protocol before functionalizing the actual devices. This is done by using a tool called Biacore 3000 (by GE Healthcare), which exploits source plasmon resonant (SPR) measurements. In order to exploit surface plasmon effect, specific type of samples are needed. They need to be covered with a noble metal layer which leads the chip's surface to be electrically conducting. In the case of Biacore chips, gold is used as selected material because it provides a good response for convenient wavelength in the visible-range [8]. Also, because it is inert in physiological buffer conditions common in biochemistry [8]. Then, the desired chemistry is deposited through the vapor phase deposition process upon the gold layer. The formed SAM will act as a dielectric layer, right above the metallic one. When polarized light hits the surface under certain conditions, electron charge density waves form right at the interface between those two materials. This happens only when the incoming radiation strikes the sample's surface at specific angles also called resonance angles, within the Total Internal Reflection (TIR) condition. TIR means that the incoming light is completely reflected, without being transmitted on the other side. In this way, free electrons of the thin gold layer absorb the energy derived by the incoming photons and convert themselves in plasmons. SPR effect depends on the refractive index of the upper material which influences both the resonance angle and the reflected light intensity. Depending on the type of molecule present on the surface, a refractive index change occurs. As a consequence, the outcome visualized on the Biacore software will change in real time. The resulting diagram is also called *sensogram*.

Biacore

Before running an experiment on Biacore tool, we need to prepare the sample and to perform a cleaning procedure of the machine. The cleaning procedure includes the flowing of two different desorb solutions within the four channels. Desorb solution 1 contains 0.5% sodium dodecyl sulphate (SDS), and Desorb solution 2 contains 50mM glycine pH 9.5. They are both provided by Bioanalytics Xantec and they represent a typical kit for cleaning fluidics instruments like Biacore. Generally, desorb procedure is carried out twice. During the cleaning procedure, Biacore samples can be cleaned using wet chemistry. Rinsing with acetone and IPA helps removing organic traces on top of the surface. Blowing with N2 is used to dry the sample before introducing it in the machine. Once the second desorb procedure is finished and the sample is ready to use, priming is performed using the desired buffer solution. In our case, 0.1x Phosphate-Buffered Saline

(PBS) solution with pH 7.4 is used. It is equivalent to say PBS solution with a salinity of 15mM. After priming, a good practice is to check the dips on the Biacore software, which indicate if the sample was mounted correctly. The dips represent the reflectivity at the sample's surface. Since four different micro-channels cover the entire sample's surface, four different dips exist depending on the channel's number. The correct dips should include four curves almost overlapping that bottom out at a reflectance value of about 10000 [26]. An example of good dips is shown in Figure 2.1.

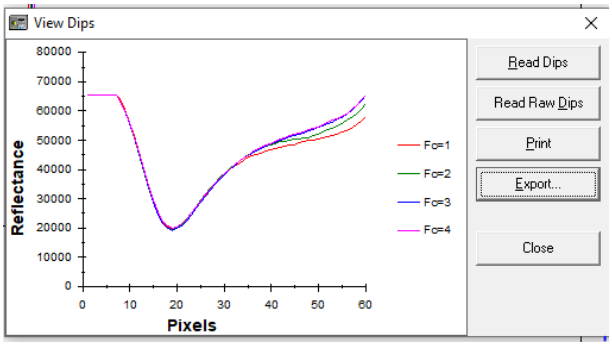

Figure 2.1: Dips in Biacore tool after priming. The overlapping of the four curves assures the correct sample's position inside Biacore tool.

Next step is to start running the Biacore method. Running experiments on Biacore tool requires a protocol for the success binding of DNA on the sample's surface. This protocol is called also *method* on the Biacore software. In our case, it includes the following steps:

- glycine (pH 2.2) injection, flow rate 20μl/s for 5 minutes, repeated two times
- glutaraldehyde (GA) injection, flow rate 5μl/s for 30 min
- oligonucleotides injection, flow rate 5μl/s for 20 minutes
- glycine (pH 2.2) injection, flow rate 20μl/s for 5 minutes, repeated two times

where oligonucleotides concentration is not standard. At the beginning, both 2μM and 5μM DNA were used, then only the former was employed. This because no improvements were noticed in the DNA density on the sample's surface for increasing DNA concentration, as it was expected. The reasoning might be that the sample's surface was already saturated at low concentration, leading to no more rooms for new oligonucleotides binding on the surface.

Apart from the DNA concentration, also different DNA molecules were adopted during different experiments. The tested molecules are:

- 50 (adenine) bases DNA oligonucleotides, sequence: 5'/NH2-C6-50A-NH2/3' with HPLC purification
- 100 bases (50 adenine and 50 thymine) DNA oligonucleotides, sequence: 5'/NH2-C6-50A50T-NH2/3' with HPLC purification

- Hairpin DNA, sequence: *GGGGTGGGGTGGGGTGGGG/iAmMC6T/TTTTTT GGGGTGGGGTGGGGTGGGGTTTTTTTTTTCCCCACCCCACCCCACCC CAAAAAAACCCCACCCCACCCCACCCC* with HPLC purification

All the listed molecules have been purchased from IDT, and they are amino modified in order to let the DNA binding with the glutaraldehyde (GA) via Mannich reactions and/or reductive amination [30]. The amino-modification is on both the terminations of the single-stranded DNA (ssDNA) because the goal is to maximize the charge near to the surface. A graphical representation of the binding strategy is represented in **Figure 2.2**.

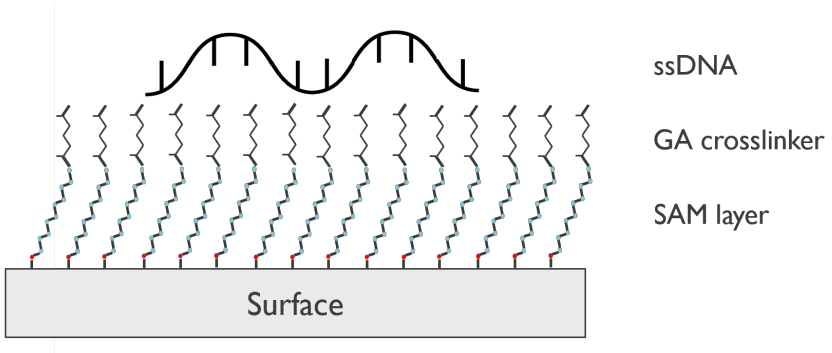

Figure 2.2: Schematic representation of DNA binding strategy. Self-assembled monolayer forms on top of the silicon dioxide surface. Glutaraldehyde binds to the amino terminations of the SAM. Eventually, amino-modified ssDNA binds to the terminal groups of glutaraldehyde molecules.

2.3 FETs fabrication

Even if the fabrication process of the finFETs used in this work is not part of this thesis, a brief general description of the selected devices is provided hereafter to understand the bioFETs structure. BioFET sensors are based on the liquid-gated technology, which means that the metal gate of the finFETs is removed to form a cavity. When filled with liquid, this cavity functions as a liquid gate. Hence, the typical fabrication process for standard finFET has to be modified to create the liquid gate. The selected devices are inversion-mode p-type FETs. Their process flow includes the fully-integration of both front-end and back-end fabrication in the 300 mm pilot line.

The finFETs are created starting from 300 mm silicon-on-insulator (SOI) wafers (Soitech). They are characterized by a buried oxide (BOX) with a thickness of 145nm, a silicon layer on top (resistivity ∼12 Ωcm) thick 88 nm and a bottom silicon layer with a thickness of 775 μm. The top Si layer is the one where the finFET structure is obtained. More specifically, a fin height of about 20-30 nm is achieved by successive steps of oxidation and wet etching processes [24]. While, different fin widths (from 1μm to 10 nm) and

gate lengths (from 10 μm to 50 nm) are derived by using an advanced patterning approach based on 193 nm immersion lithography and hard mask shrinking [15]. Before growing the 4nm thick thermal silicon dioxide layer on top of the wafers, a fin cut step modifies the devices to obtain single-channel FETs [15]. For what concerns the doping, the n-type Si layer forming the channel was slightly doped ($N_D = 10^{17} cm^{-3}$). While, the dopant density in the p-type drain and source regions was made quite high (larger than $N_A = 10^{20} cm^{-3}$). The gate terminal was initially grown as a polysilicon layer, also called dummy gate, with a thickness of 80nm. After the gate patterning, the devices were annealed at a temperature of 1030 °C to improve the silicon-silicon dioxide interface quality and activate the dopants [24]. At this point, the front-end of the line is terminated.

The back-end of the line starts with a deposition of 200 nm thick silicon dioxide as passivation layer. Afterwards, the drain and source contacts are created on top of the passivation layer, and they are connected with the downer part of the device thanks to tungsten vias. Consequently, the metal interconnections have to be passivated to avoid the electrolyte solution being in contact with the metal. For this reason, a 300 nm oxide layer is deposited on top. Eventually, the cavity is open by means of a combination of dry and wet etch processes [24]. The last two steps consist in the deposition of aluminum as drain and source metal contacts first. Then, the deposition of a photoresist over the entire wafer ends the process. It is done to protect the devices before using, particularly during the dicing and manipulating process. The result are finFETs with a cavity of approximately 1 μm high, 2 μm wide and a length equal to the dummy gate length [24]. Before functionalizing the finFETs, the photoresist was removed using hot micro-strip at a temperature of 75°. Moreover, the dies received a cleaning procedure with UV/O3 for 15 minutes to remove left-over organic contamination. The total process flow for bioFETs creation ends with a forming gas annealing (FGA) to restore the good quality of the oxide-semiconductor interface that degrades after the UV/O3 step [24]. The final result are bioFETs chips called also bare oxide devices, that need an immobilization process before detecting biomolecules. The complete process has been already explained in detail in Sec. 2.1.

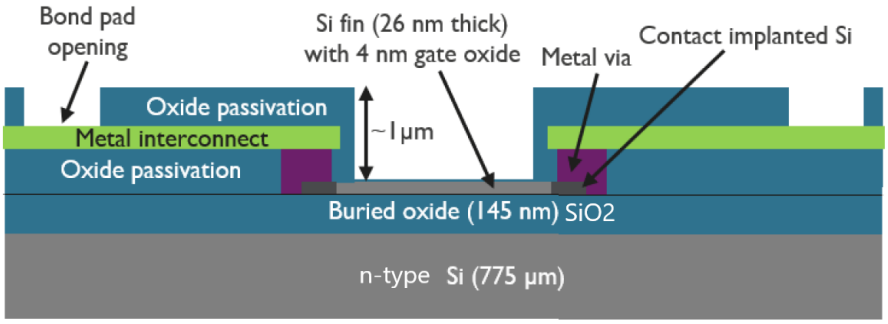

Figure 2.3: Cross-sectional schematic of bioFETs fabricated using finFET technology. The figure is readopted by Figure 12 in [24].

2.4 Molecule binding protocol

In this section, the binding of target molecules to the FET surface is explained more in detail. The target molecule chosen in this thesis work is single-stranded DNA. As already stated before, different kinds of ssDNA oligonucleotides have been analyzed. Their difference consist in the type of nucleotide sequence they form, which will give rise to different charge redistribution. As a result, when DNA binds to the functionalized FET surface, different currents will be generated depending on the type of molecule. However, each DNA sample has been synthesized with amino modifications at both the 5'-end and 3'-end of the oligonucleotides. Therefore, the binding procedure will follow always the same protocol.

The binding procedure starts from the silanization of the surface by performing vapor-phase deposition of APTMS. Binding of silicon-based molecules (like APTMS) on metal/oxide surfaces (in our case, SiO2) occurs because hydroxyl groups (-OH) can easily link to silicon atoms. Then, glutaraldehyde (GA) molecule binds to the amino-termination of APTMS via Mannich reactions and/or reductive amination [30]. Consequently, the amino-termination of the target molecule binds to the other formyl group of GA. More specifically, GA is used as a crosslinker agent to allow the controlled binding of DNA to the surface by means of the aminoalkylsilane functional layer. **Figure 2.4** represents the binding protocol of the target molecule to the surface by means of APTMS functional layer. In the case of AUTES chemistry, the strategy is exactly the same.

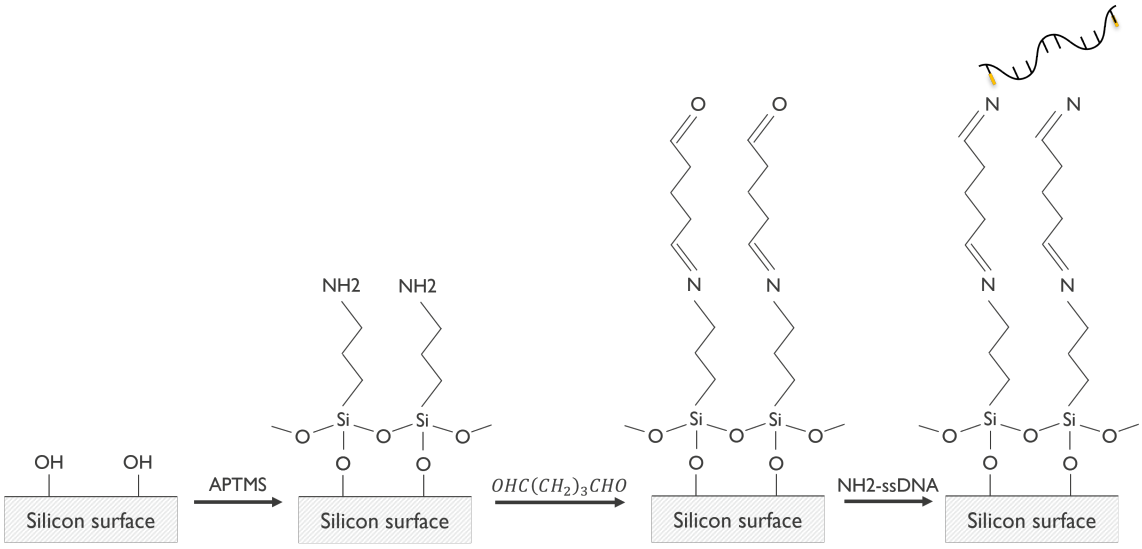

Figure 2.4: Schematic representation of the functionalization procedure on FET surfaces. DNA binding occurs by covalent bonding of amino-modified ssDNA with a silane coupling. First, APTMS binds with silanol groups. Then, glutaraldehyde works as crosslinker agent between both NH2 terminal groups of APTMS and DNA molecule. The amino termination of DNA is shown in yellow.

2.5 bioFET characterization

In this section, we will discuss the methodology and protocols used for the electrical characterization of the functionalized bioFETs. In particular, there is a first part about the techniques generally used for conventional FETs. Then, the methodology used for this specific kind of bioFETs is illustrated later.

2.5.1 Electrical measurements on FETs

The working principle of bioFETs has been already discussed in Sec. 1.1.3. In particular, it has been shown that bioFETs are identical to whatever type of solid-state FET, expect for the liquid-gated technology. Therefore, the general description for the implementation of electrical measurements on solid-state FETs has to be explained first. Then, additional components especially needed for the characterization of bioFETs are included in the general description.

At Imec, the electrical characterization of solid-state FET is carried out on the PA300 nano Probe station (by SUSS Microtech). It is a semi-automatic electro-mechanical tool for the testing of wafers with a diameter up to 300nm. In our case, we do not use an entire wafer at a time, but we use a single die where more than 100 devices are present. In order to perform the measurement, the chip is placed at the center of a metallic plate called chuck, which acts as a back gate. The chuck can be moved thanks to a controller through a joystick. Other two fundamental components of the Probe station are the probes and the microscope. Each probe has a metallic needle that creates an electrical connection with the source and drain pads of the transistors, after they are put in contact. The microscope is fundamental to achieve this goal because the pads are just some micrometers long and they are impossible to see with naked eyes. However, before creating the contact we need to align the wafer. This is a very important step because the chuck automatically moves upon different devices on the chip by means of a *Perl* script. The script is in charge of the communication between the probe station and the source-measurement unit (SMU). The latter is the tool that is performing the real electrical measurement. In particular, we use the Keithley 2602 tool as source meter. Actually, since each device is composed by four terminals (source, drain, gate and back gate), we use two Keithley tools, each of them containing two SMUs. In this way, we can obtain information about all the relevant voltages and currents in the circuit. The most relevant ones are: the source-to-gate voltage (V_{GS}), the source-to-drain voltage (V_{DS}), the drain (I_{DS}) and the gate current (I_{GS}). Ideally, the last one should be null.

2.5.2 Fluidic setup

Since we are dealing with bioFETs based on liquid-gated technology, a fluidic setup is needed in order to perform the electrical measurements. In particular, the type of fluidic setup used in this thesis work is called pressure-driven set up. It includes a pressure controller whose inlet is a pressure of 2 bar maximum. The pressure can be adjusted in the whole range till 0 bar thanks to the *OxyGEN* software. The desired pressure is sent

to a certain number of liquid reservoirs, which are also connected to a switcher. The switcher can be controlled via software to choose the specific liquid. Then, the selected fluid passes through a degassing chamber that is needed to avoid bubble formation in the micro-channels. Bubbles can either reduce the flow rate during the experiment or clog the channels in the worst case. Moreover, bubbles at the micro and nanoscale are very difficult to remove due to surface tension effect. So, the use of a degasser is really recommended. The output of the degasser is connected to the flow cell mounted on the chip to be analyzed. While, the other part of the flow cell is connected to a T-connector. The vertical part of the T-connector hosts the reference electrode, while the other extremity is connected to a flow unit. The latter is responsible for the flow rate determination. The reference electrode is formed by a Ag/AgCl wire immersed in a 3M KCl solution. It determines the constant reference voltage useful in the expression of the threshold voltage of the transistor. Eventually, the flow unit is connected to a waste container, where the fluid will end up to. The complete set up is shown in **Figure 2.5**

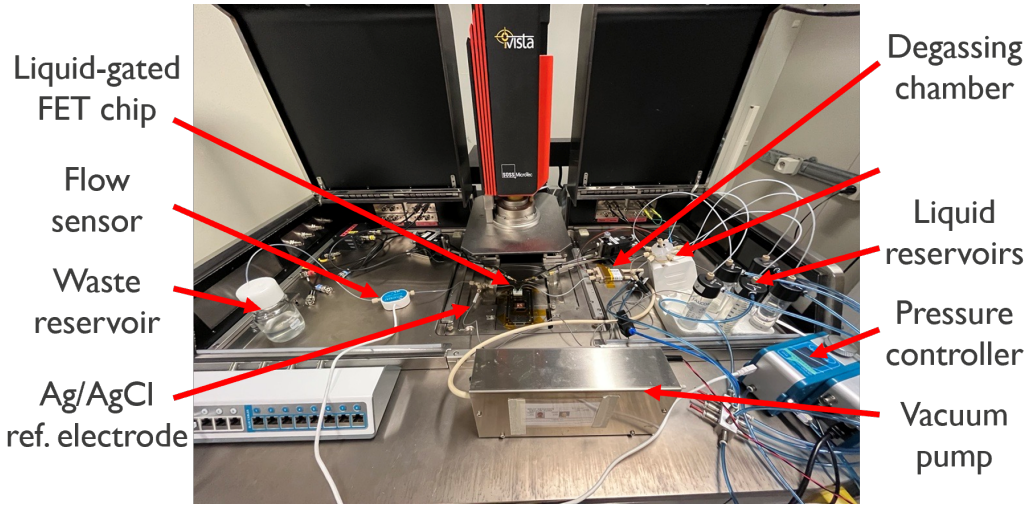

Figure 2.5: Pressure-driven fluidic set up.

2.5.3 Priming and wetting procedure

Once the fluidic setup is completely mounted, a priming procedure is needed before starting the electrical measurements. In particular, it is useful to be sure that the circuit is well-mounted and no clogs are present in the micro-tubes. The priming procedure includes the flushing of 100% isopropanol (IPA), a mixture of 50%IPA and 50%buffer solution, 100% buffer solution, glutaraldehyde (GA), DIW and air. Each one of these liquids is flushed for about 4 min at a constant pressure of 1000 mbar. Particular attention is dedicated to the first passage of the liquid after the degasser. Its presence is also confirmed by the flow unit, which will report an increase of the flow rate after the liquid passed through it. It is important to underline that during the priming procedure, the flow cell is not mounted yet. It is simply replaced by a tube, whose only function is to

create a closed circuit.

After the priming procedure is finished, the flow cell can be connected between the degasser and the reference electrode. A procedure similar to the priming one can be performed. It is called wetting procedure and it consists in the flushing of the following fluids: 100% IPA, a mixture of 50% IPA and 50% buffer solution and finally 100% buffer solution. During these steps, the devices on the bioFET chip are filled in with the liquids, implementing the liquid-gated technology principle. Particular attention is given to the passage of the liquid throughout the flow cell during this process step, because the correct mounting of the flow cell is verified by the absence of leakages.

Next, the contact between the device and the electrical probes can me made by following the protocol of the probe station. The physical contact between the probes' needles and the devices' pads guarantee the implementation of the electrical characterization. In particular, $I_{DS} - V_{GS}$ measurements are performed on the devices present on the bioFET chip by means of *Perl* scripts run from the terminal. $I_{DS} - V_{GS}$ measurements are useful to extract the FET properties, like threshold voltage and subthreshold swing. These parameters help to choose the best device to be selected for biomolecule sensing. During the entire electrical characterization, the flow rate is set to 25μL. This means that whatever type of liquid is injected into the system, the pressure is modified accordingly to still have a flow rate equals to the chosen one. Hence, the pressure can change during the experiment. Specifically, if the fluid is denser the corresponding pressure will be higher.

2.5.4 Protocol for bioFETs characterization

The measurement protocol for the sensor characterization includes a first $I_{DS} - V_{GS}$ scan among all the devices present in the chip. It is useful to check whether the devices are effectively working or not. In this first *Perl* script, a double gate voltage sweep is performed. It means that the drain voltage is kept fixed at $V_{DS} = -0.1V$, while the gate voltage is changing back and forth between $V_G = 0.2V$ and $V_G = -1V$, with a step of $V_G = 0.02V$. A double sweep is needed to avoid damage to the devices caused by electrostatic discharge. More in detail, when the voltage is quickly released after it reaches the maximum in absolute value [24]. As a consequence, two $I_{DS} - V_{GS}$ curves are extrapolated for each device: the first one is obtained going from higher to lower gate voltages, while the second one is obtained in the reverse condition. Theoretically, the two curves should be coincident, but sometimes they are not. In this last case, we talk about hysteresis of the curves.

Consequently, about 25 devices are chosen among the ones which are correctly working. The criteria to understand the best devices to work with are the steepness of the $I_{DS} - V_{GS}$ curve and the absence of hysteresis. After choosing the best devices, a first stability test is performed on them by using a second *Perl* script. This time, each device is analyzed five times to check their reliability on time. Furthermore, the gate voltage range is decreased between $V_G = -0.4V$ and $V_G = -0.1V$, in order to focus on the under-threshold region. The results are five graphs for device, each of them containing two $I_{DS} - V_{GS}$ curves (ideally, overlapped). The best device in term of reliability is

represented by the one whose $I_{DS} - V_{GS}$ characteristics do not change among the five repetitions. This criterion is checked by looking at the gate voltage in correspondence of $I_{DS} = 1nA$. If the relative gate voltage is changing in the range of mV, the device is considered to be good.

Among the 25 devices analyzed for stability, only one has to be chosen for the real-time measurement. The criteria are the ones already listed before: steepness of the curve, absence of hysteresis and invariance of the gate voltage in correspondence of $I_{DS} = 1nA$. The selected device is analyzed with a third *Perl* script to perform a so called timetrace analysis. It consists in a real-time measurement of the I_{DS} versus time, at fixed drain voltage and fixed gate voltage. The drain voltage is always assumed equals to $V_{DS} = -0.1V$, while the gate voltage is not decided a priori. Indeed, its value depends on the parameters of the selected device extracted in the previous steps. In addition, since the binding protocol includes a two-steps process, more than one timetrace analysis are carried out. Among them, the integration time is not always the same. Therefore, both gate voltage and integration time parameters are modified in the *Perl* script ad hoc, depending on the type of device and binding molecule.

Stability study and timetrace measurements are repeated in sequence three times. The protocol includes a first stability test to choose the selective device to be analyzed during the entire experiment. Then, a first timetrace measurement is performed during the glutaraldehyde (GA) injection. The GA works as a crosslinker between the functional layer and the target molecule. After that, a new stability test is carried out to be sure that the selective device is still working. Before performing the timetrace measurement relative to the analyte, a new timetrace is executed. It is performed during the injection of the buffer solution only, also called dummy sample. This step is important to set a new baseline before the DNA detection. Indeed, the analyte has been suspended in the same buffer solution than the dummy one. Thus, potential differences in the timetrace curve could be assigned to the presence of the target molecule only. Also in this case, before performing the DNA timetrace, a new stability test is carried out. It is needed to be sure that the chosen device is working correctly. The experiment ends with a last stability test performed after the flushing of DNA. It is useful to analyze possible differences in the FET parameters after the biomolecule detection.

Chapter 3

Surface engineering: SAM optimization

In this chapter, the experimental results concerned the chemical characterization of the aminoalkylsilane self-assembled monolayer (SAM) are shown and discussed. They are obtained by following the exact procedures outlined in Chapter. 2. In particular, the results of each characterization technique applied to both APTMS and AUTES coatings are reported at once. This working flow is effective to obtain a clear comparison between the two coatings in terms of contact angle, thickness, surface charge and binding capability. At the end, based on this information, the best chemistry to be deposed on bioFETs has been chosen.

3.1 Experimental results and discussion

One of the most important aspects in engineering is the reproducibility of results. Therefore, the deposition process has been repeated many times for each kind of chemistry. The goal is to understand the quality of the new surface coatings, that will work as functional layers for our bioFET sensors. In the following, just the results of few repetitions are reported for each characterization technique. Further data can be found in the appendix.

3.1.1 Contact Angle

Static contact angle measurements are the first ones implemented right after the vapor-phase deposition process. They are performed through a OCA 20 contact angle system (DataPhysics), using DIW as dropping liquid. A typical measurement on *SCA20* software appears like the one represented in **Figure 3.1**. There, it is highlighted how the software automatically calculates the wetting angles between the droplet of DIW and the sample's surface. Two angles are reported for each measurement: CA left and CA right. They correspond to the left and right part of the droplet seen as a two-dimensional bead from the lateral side of the camera. The two results are averaged with the other ones obtained in different points of the sample's surface. In **Figure 3.2**, the averaged CA values for both APTMS and AUTES coatings are reported.

Figure 3.1: Example of a contact angle measurement on *SCA20* software.

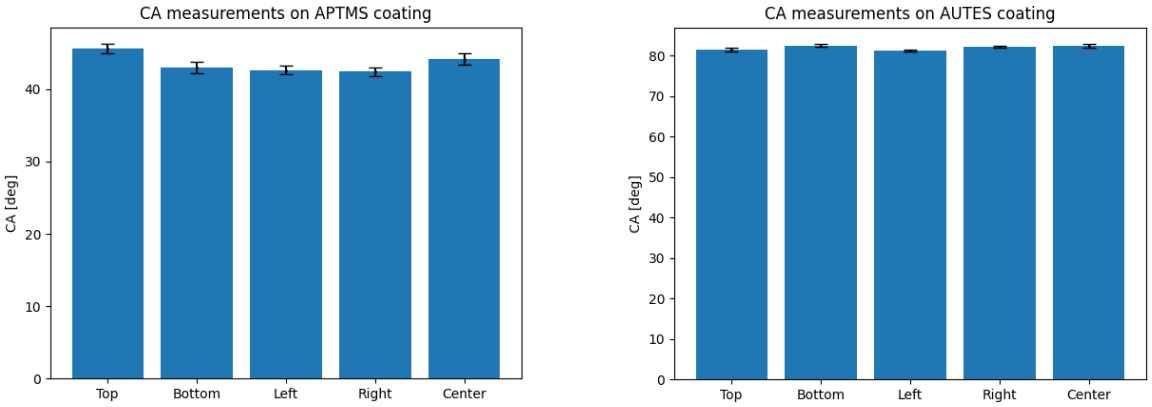

(a) APTMS

(b) AUTES

Figure 3.2: Each column represents the average of five CA measurements taken on different positions of the sample's surface. The error bar in each column represents the average standard deviation among the five measurements.

By looking at the results, it can be noticed how the surface is more hydrophilic after the deposition of APTMS chemistry because the contact angle is always smaller than 50°. While, in the case of AUTES coating, the surface is much more hydrophobic, with a contact angle about 80°.

As first analysis, the APTMS coating seems to be better for applications in nano-scaled bioFETs because of its characteristic to be more hydrophilic. More specifically, when working with liquid-gated technology at the nano-scale, it is important to consider that some factors may become relevant. One of them is the wettability of the surface, a characteristic that is effectively represented by the contact angle. In particular, the lower the

contact angle and the higher is the probability that the liquid will fill homogeneously in the cavity. As a result, if a nano-scale device has a higher wettability there will be more chances for a macromolecule to bind to the functionalized surface. Hence, the bioFET signal will be higher and the sensor response will be boosted.

3.1.2 Ellipsometry

Thickness value is another important parameter for the characterization of the SAM. It determines the minimum distance between the target molecules and the FET surface. Also, thickness measurements allow to discover homogeneity in the vertical growth of the functional layer. In our case, the recipe used in the *CompleteEASE* software of the ellipsometer tool includes a nine-points scan pattern. It follows a snake-like path and it represented in **Figure 3.3**.

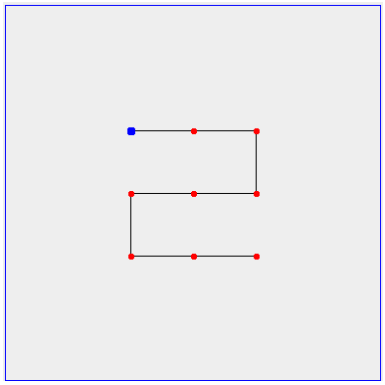

Figure 3.3: Scan pattern for ellipsometry. Blue line represents the samples' border. Red points represent the measurements points. Black lines represent the path that the light is crossing to evaluate a new measurement point.

In **Figure 3.4**, thickness measurements for both APTMS and AUTES coatings are shown. The results are simply obtained through the software as a series of fitted thickness value and mean squared errors (MSE). By looking at the results, the aminoalkylsilane groups seem homogeneously distributed among the samples' surfaces due to the almost identical results for all the analyzed cases. This outcome confirms that the samples' location within the desiccator does not affect the SAM's properties.

By looking at the results, the thickness of the APTMS coating is more than doubled with respect to the AUTES one. With equal blanket's thickness, the average APTMS thickness is about 1.77 nm, while the one of AUTES is about 0.84 nm. This outcome could be the result of the higher polymerization capability of APTMS, maybe caused by the intrinsically shorter aminoalkylsilane chain that helps the molecules' rearrangement. By doing some trivial calculations, the length of APTMS molecule seems to be around 8Å. This is consistent with [1], where it is reported a molecule's length for 3-Aminopropyltriethoxysilane (APTES) ranging from 5Å to 10Å. The previous calculation is based on the idea that molecules will lie perpendicularly to the surface, but the real

molecules' arrangement could be different. For example, an angle between the surface and the bulky group of the SAM may be formed. As a result, the effective length of the molecule will be smaller. Also, it may happen that the chemistry polymerizes forming more than one single layer, resulting in a thicker functional layer. This last assumption paves the way to a very important question: will the (NH2) terminal groups of the aminoalkylsilane coatings be still present to functionalize the surface after the polymerization? To answer this question, it is fundamental to analyze the surface's activation by means of Fourier Transform InfraRed spectroscopy (FTIR), before discussing the best chemistry in terms of thickness. In principle, the thinner the functional layer and the better is the sensor response. At least, for bioFET applications. That is because we are working with charged surfaces and electrolyte solutions, which always give rise to an electrical double layer (EDL) formation. As already stated before, the EDL is characterized by the Debye length, which eventually contributes to set the sensor's detection limit.

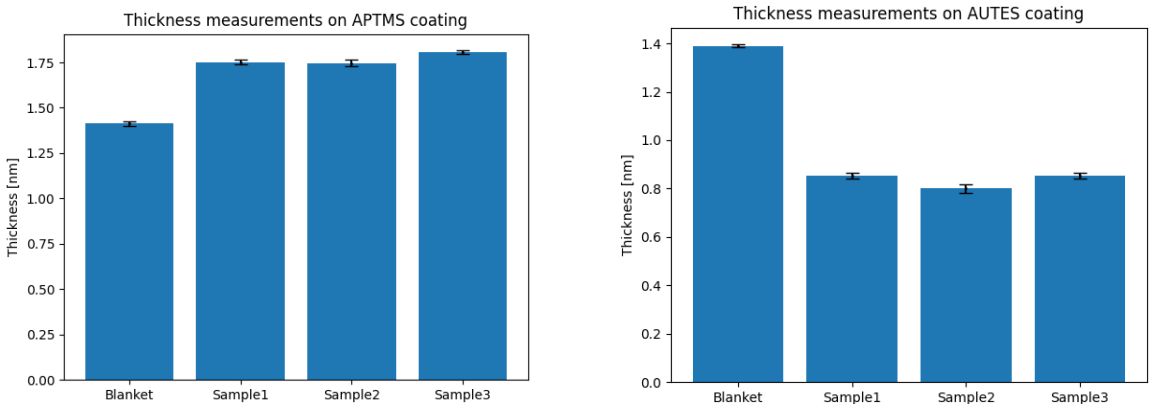

(a) APTMS

(b) AUTES

Figure 3.4: Each column represents the average of the nine-points measurements. The error bar in each column represents the average standard deviation among them. Sample1, Sample2 and Sample3 refer to three different samples' location within the desiccator.

3.1.3 FTIR

Surface activation has been analyzed thanks to Fourier Transform InfraRed spectroscopy (FTIR) measurements. FTIR results are shown in **Figure 3.5** as a series of graphs representing the absorbance versus the wavenumbers. Each absorbance peak highlights the presence of a specific chemical species or type of binding. In the case of aminoalkylsilane coating, the relevant peaks are the ones relative to the NH2 terminal groups and the residual unbound SiO2 groups at the Si surface. According to the FTIR manual [18], Amine N-H deformation vibrations-saturated primary amines-have absorption between 1580 and 1650 cm^{-1}, Amine hydrihalide N-H3+ deformation have absorption between 1585 and 1560 cm^{-1} and Amine hydrihalide N-H2+ deformation have absorption between 1620 and 1560 cm^{-1}. Therefore, the wavelength window we are interested in to check

the presence of NH2 terminal groups is almost the one between 1600 and 1500 cm^{-1}. While, the Si-O-Si asymmetric stretching vibration band is normally between 1100 and 1000cm^{-1}.

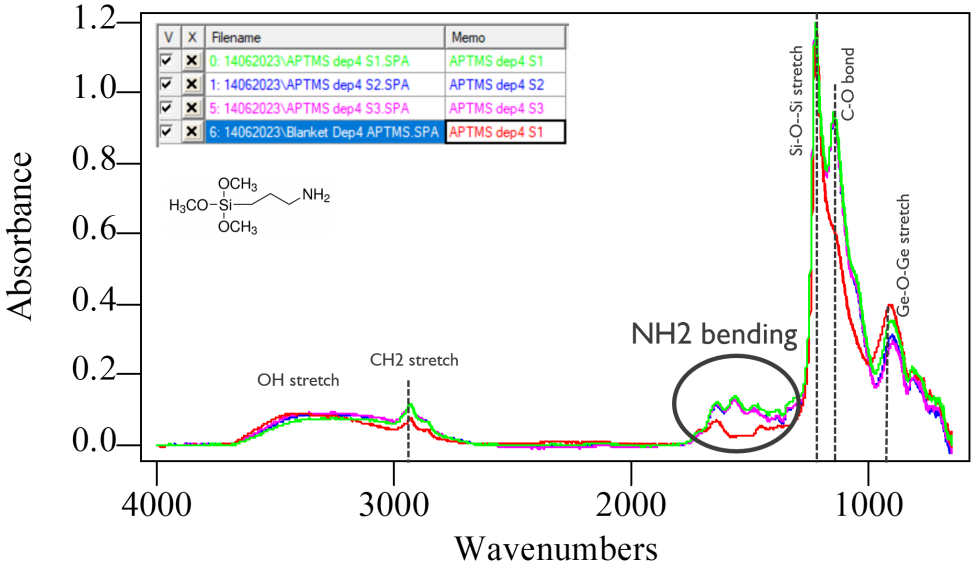

(a) APTMS

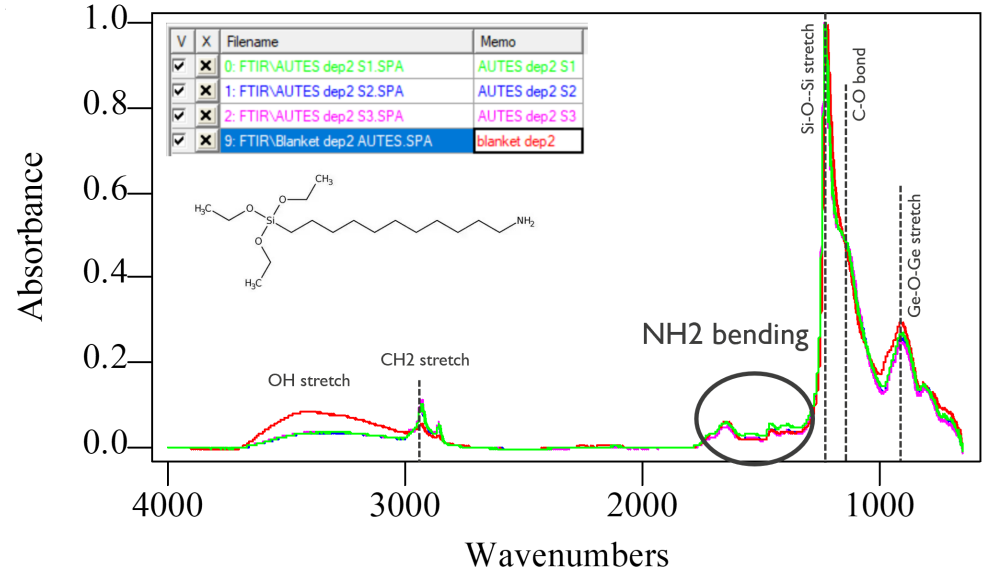

(b) AUTES

Figure 3.5: Absorbance spectra of APTMS and AUTES coatings as a result of FTIR measurements.

First, the results show that the Si-O-Si peak is always present, both in the blanket and

in the coated samples. This outcome suggests that in any case the surface is not fully covered by the chemistry after the deposition process, since some residual silanols groups are detected by the FTIR. For what concerns the amount of chemistry, in the case of APTMS a well defined absorbance peak is found in correspondence of the NH2 window (between 1600 and 1500 cm^{-1}), while in the same region the blanket spectrum is completely flat. Moreover, the presence of NH2 groups at the surface seems to be nearly the same in all the analyzed samples because of the almost coincident APTMS spectra. However, no quantitative information about the surface density of APTMS can be obtained from single FTIR analysis. The amount of amino groups can be evaluated just as a comparison between previous FTIR results, stating whether it is higher or lower than previous values. To this aim, the creation of comparative histograms is carried out by collecting the absorbance peak of the amino groups. Both from different samples and deposition processes. Even if the results are not quantitative, this task may help in understanding the reliability of the deposition process. In **Figure 3.6**, the results for the APTMS coating are reported.

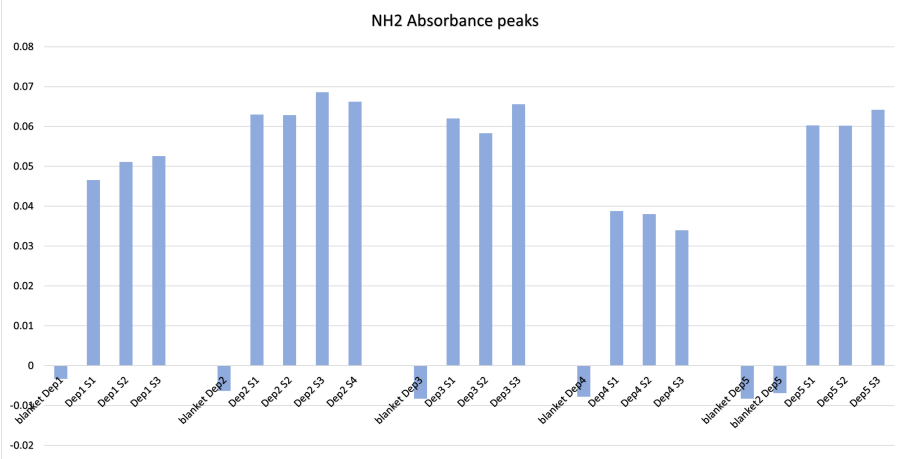

Figure 3.6: Comparison of NH2 absorbance peaks of APTMS coatings. Three samples have been analyzed within the same deposition process. They differ only for the location within the desiccator. The same analysis has been repeated five times.

In the case of AUTES, the situation is quite different because the absorbance peak related to amino groups is not clear-cut. As shown in **Figure 3.7**, only some bumps can be noticed in the absorbance spectra within the NH2 range (between 1600 and 1500 cm^{-1}). In addition, there is not a well-defined difference between those bumps and the almost flat region in the blanket's spectrum.

On first impression, it may seem that no amino groups are present on top of the surface. However, all the others characterization techniques confirm the presence of AUTES molecules on top of the oxide surface. Therefore, it is likely that amino groups are present on the surface, but they are arranged differently from what was expected. For instance, it

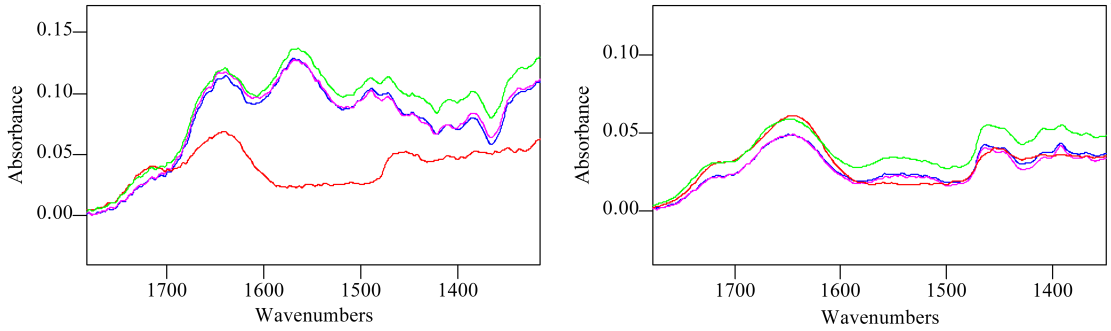

(a) APTMS (b) AUTES

Figure 3.7: FTIR results: zoom on amino groups.

may happen that the NH2 groups do not stand perpendicular to the surface and the FTIR tool does not detect them. Indeed, as reported in Sec. 2.2.4, we use p-polarized light to analyze the functional layer. By definition, p-polarized light means parallel to the plane of incident and perpendicular to the surface. When measuring with p-polarized light, the x and z components of the IR light probes the film [17]. While, the y component probes the film in the case of s-polarized light (**Figure 3.8**). Hence, a different SAM orientation (not strictly vertical) would have been pointed out perhaps by using s-type polarization setting in the ATR-FTIR tool. Future works could implement a similar analysis.

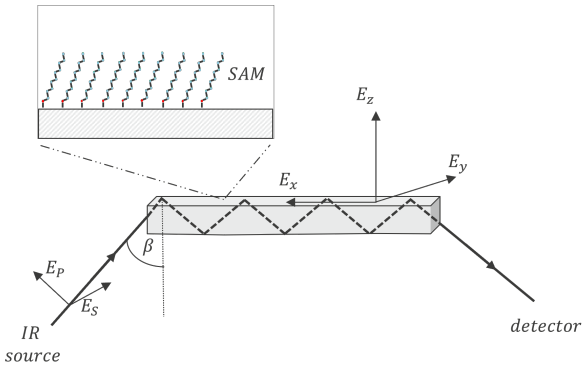

Figure 3.8: P and S type polarization in ATR-FTIR technique on SAM-coated samples.

3.1.4 Surface Potential

The surface charge after the silanization process has a great relevance for biosensing purposes. Indeed, since bioFETs are based on a liquid-gated technology, an electrolyte solution is always involved in the process. This means that an electrical double layer (EDL) will be formed at the boundary between the surface and the fluid. Therefore, we need to understand the role of the chemistry in the surface charge modification.

As already discussed in Sec. 2.2.3, the streaming potential tool is one of the possible

way in which we derive the surface charge. Actually, an exact surface charge derivation is a quite difficult goal to achieve, since the parameters involved depend on the pH of the solution that is not constant. Therefore, the analysis concerning the surface charge on top of the SAM will be indirectly accomplished by looking at the surface potential results and comparing them to the general formula:

$$\sigma_e = \frac{\sigma_c \zeta \lambda_D}{D} \tag{3.1}$$

where σ_e is the surface charge, σ_c is the electrical conductivity of the fluid, ζ is the zeta potential, λ_D is the Debye length and D is the diffusivity. The relationship between surface charge density and zeta potential defined in **Equation 3.1** is simply derived by using the charge conservation law. The relevant information deriving from the previous formula is the sign of the surface charge, which will be in accordance with the sign of the zeta potential obtained from the surface potential measurements. For instance, if the surface potential results to be greater than zero, the surface can assumed to be positively charged, and vice versa. In **Figure 3.9**, a couple of results for both APTMS and AUTES surface potential measurements are reported. A pH range between 3 and 11 has been analyzed.

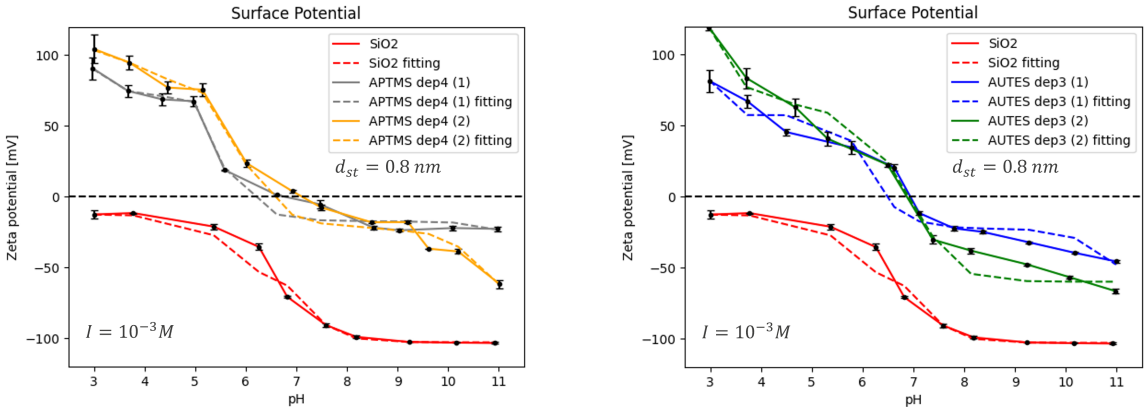

(a) APTMS

(b) AUTES

Figure 3.9: Surface potential results. (1) and (2) refer to different samples within the same deposition process. I indicates the ionic strength of the solution used during the experiments. d_{st} is the thickness of the Stern Layer used for the fitting in the *Python* simulation. The value has been extrapolated based on [28], considering *I=1mM*.

Results are represented as barplot graphs, where the error bars represent the standard deviation between four measurements performed at the same pH value. Continuous lines are used to join different measurements points. Broken lines represent the data interpolation performed by using the EDL theory, explained in detail in Sec. 2.2.3. First of all, it is relevant to highlight that similar experimental results are a novelty in the field of self-assembled monolayers, because they are missing in any official website resources so far. For this reason, especially in this case a great importance is given to experiments'

repetitions, which are fundamental to study the reliability of SAM's properties. Further repetitions can be found in Appendix A.

The first sample to be analyzed is the blanket. The bare oxide surface acts as a reference for the analysis of aminoalkylsilane SAM. In principle, all the silanols groups are available at the surface without performing any coating procedures. When in contact with water-based solutions, acidic groups like silanols dissociate producing negative surface charges by means of EDL principle. As a result, following **Equation 3.1**, the surface potential has to be negative, and this is confirmed by the experimental results. Moreover, since pKb values for the deprotonation reaction of silanol groups range from pH 4.5 to pH 8.5 [24], for pH values outside this range the curve is well-characterized by flat regions. In particular, for pH values lower than 4.5 the resulting plateau is also call isoelectric point (IEP). In that region, the surface approaches the neutrality condition and the zeta potential is almost zero.

For what concerns the other curves present in **Figure 3.9**, they constitute the surface potential measurements performed on samples coated with aminoalkylsilane SAMs. In principle, considering a fully covered surface and an ideal SAM structure, the results should depict the behavior of amino groups only (NH2). It means that the curves should lie all above the zero volt axis due to the intrinsic characteristic of amino groups. By nature, they become protonated when in contact with water-based solutions, leading to positively charged surfaces. Furthermore, since the pKa of aminoalkylsilane is reported to be around 7.6 [2], the plateau obtained for higher pH values should represent the region where almost no NH2 groups are protonated. As a result, for high pH values the surface should reach the neautrlity condition. However, results in **Figure 3.9** show that the real behavior of aminoalkylsilane SAMs is different from the expected one. The curves are shifted towards positive values of zeta potential, but not completely. The measurements performed at higher pH continue to be characterized by negative voltage values, associated to a negative surface charge. The reason for this trend could be the presence of uncovered silanols groups at the surface. Since SiOH groups are deprotonated at higher pH [23], they may contribute to the permanence of negative charges.

In the specific case of APTMS, two well-defined flat regions can still be observed. In corresponding of those pH values, the zeta potential is stable and a binding protocol would be more effective. However, other factors influence the binding effectiveness, like the value of the surface charge. As already stated before, the best surface charge for favoring the binding with negative charged biomolecules (like DNA) is a slightly positive one. By looking at the APTMS results, none of the two plateau regions is characterized by a slightly positive charge. Therefore, a trade off in choosing the best operating region has to be accomplished.

For AUTES coating, the behaviour is even more different from the ideal one, because not well-defined plateau regions are detected for any of the analyzed pH values. The region where a rapid change in the ionization state of NH2 groups occurs seems to occupy

the entire pH range. Nevertheless, thanks to the Gouy-Chapman-Stern fitting model, a flat region arises in the representation. However, the most relevant outcome from AUTES measurements is that the surface is still negatively charged at higher pH values. Even more than in the APTMS case. This result is opposite to what you expect from the molecular structure of AUTES. Indeed, a longer carbon chain within the molecule should provide more intense Van Der Waals forces between the bulky groups of the SAM. Creating theoretically a better organized layer. As a consequence, the presence of more compact NH2 groups at the top of the surface could overcome the effect of SiOH groups at the bottom.
In practice, negative charges are still present at the surface for high pH values, as shown in **Figure 3.9(b)**. The result is in agreement with the FTIR ones, which do not show the presence of higher NH2 peaks for AUTES coating. Hence, the two characterization techniques reveal consistent results. Surface potential measurements confirm the presence of amino groups on the surface, while FTIR measurements reveal a different SAM orientation that perhaps facilitates the exposure of unbound SiOH groups. To sum up, based on the results of surface potential measurements, the APTMS coating seems the best choice. Even if it does not own the perfect characteristics, it is the most reliable to be deposited on bioFET sensors.

3.1.5 SPR

The last characterization technique useful to study the property of aminoalkylsilane coating on bare oxide samples is the Surface Plasmon Resonance (SPR) technique. Biacore 3000 is the tool used in Imec to exploit this technique. It allows to investigate the binding protocol that will be carried out on the real bioFETs during the electrical characterization. The protocol and the methodology have been already explained in Sec. 2.2.5. Here, the outcomes of Biacore tool are reported in the form of sensograms. Sensograms are plots of response (Response Unit, dimensionless) versus time (in seconds, [s]) that show the results of the interaction between different molecules during the running *method*. Changes in the RU have to be attributed to the formation or the dissociation of a chemical bond at the surface level. Both processes modify the surface's refractive index and can be detected by the SPR technique.

Each curve in the graph represents a different fluidic channel under the sample's surface. Each channel follows the previous one in a sort of snake-like pattern. The only difference is their position under the sample's surface. In principle, only one channel would be enough to test the binding protocol. But, thanks to the activation of all them it is possible to verify the uniformity of the coating. In particular, the RU value related to the binding of oligonucleotides is extracted from each curve. Then, their values are collected in the form of histograms. Theoretically, for a single sample the RU values obtained from the four channels should be the same. This would indicate the good conformity of the sample's surface. In practice, a variation within the results is always present. But, it is not always due to the not homogeneity of the surface. For instance, **Figure 3.11** shows the results for the binding protocol with AUTES coating. In this case, a malfunction in the first channel is clearly evident due to the random behaviour

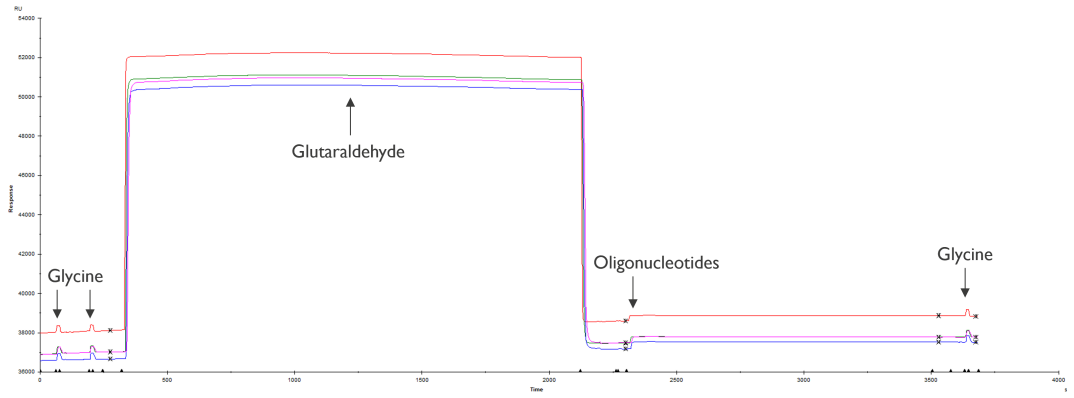

Figure 3.10: Biacore results for APTMS coating. Channels are listed as: 1 (red), 2 (green), 3 (blue) and 4 (pink). The buffer solution is 0.01x PBS. The *method* includes: injection of 10% glutaraldehyde (GA) for 30min and 20min injection of 2μM 50A ssDNA in 0.01xPBS.

during the glycine injection. This was indeed a certified problem of the tool, which has been solved by other users lately.

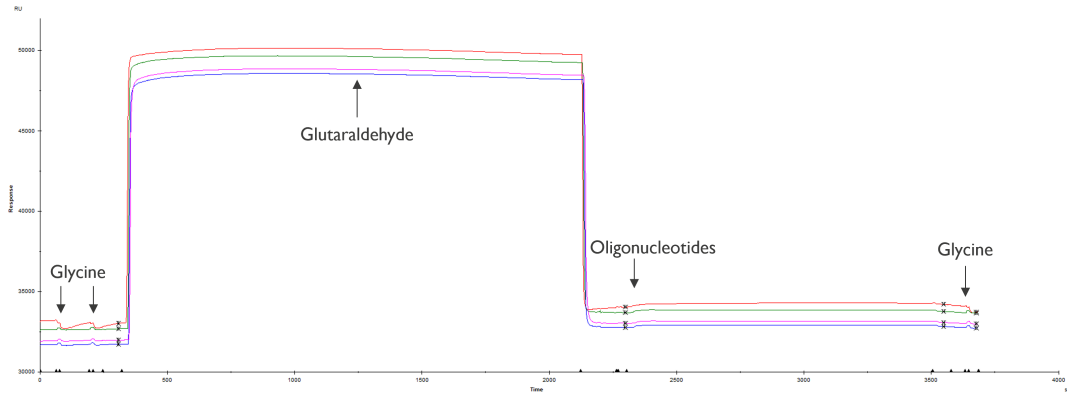

Figure 3.11: Biacore results for AUTES coating. Channels are listed as: 1 (red), 2 (green), 3 (blue) and 4 (pink). The buffer solution is 0.01x PBS. The *method* includes: injection of 10% glutaraldehyde (GA) for 30min and 20min injection of 2μM 50A ssDNA in 0.01xPBS.

By following the time axis in Biacore sensograms, different events occur. First of all, two initial pulses highlight the presence of glycine within the channels. Glycine is just used as further cleaning agent before waiting for the binding protocol to start. By following the trend of one single curve in **Figure 3.10**, no changes in the RU are visible before and after the glycine pulses because glycine does not bind to the surface. After that, glutaraldehyde (GA) is injected in the channels for 30 minutes. The RU rises up a lot because the concentration of GA is quite high (10% in DIW). However, after 30 min injection the curve ramps down because the flow of GA molecules ends. Just a few of them binds to the NH2 groups at the surface. In principle, each amino group of the functional

layer should bind to a GA molecule. The new baseline is taken just few ms before the DNA injection to be sure that the curve is as much stable as possible.
The most relevant part of the sensogram is the binding of the amino-terminated oligonucleotides to the formyl groups of GA. The transient during the molecule binding is shown in detail in **Figure 3.12**. The RU values listed in the table next to the graph are taken after around 20 minutes from the injection of DNA. 20 minutes is the time in which DNA is flowing in the channels and the signal is maximum. When the flow of DNA stops, a little drop in the RU occurs. That is the time chosen to collect the DNA signal. This detail can be noticed by looking closer at the last part of the full-range sensogram. Such behavior can be related to DNA molecules bound to the surface by means of electrostatic interaction or Van Der Waals forces, instead of chemical bonds. Those molecules can not be counted in the binding protocol procedure because they are flushed away immediately after the following buffer injection. Therefore, the RU values referring to oligonucleotides are always taken after this reduction, in order to take into account only the molecules effectively bound to the surface. The protocol ends with a last glycine pulse, but it is not relevant for our purposes.

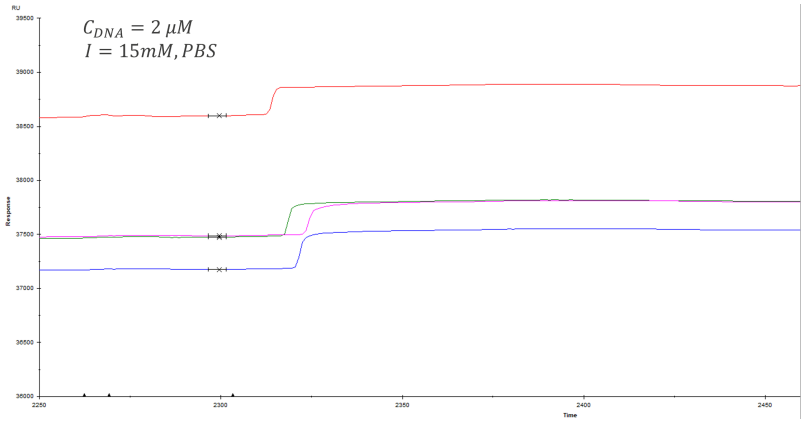

Oligos immobilization:
50A

Channel	RU*	DNA density [DNA/cm2]
1	267.3	1.02E+12
2	309.4	1.18E+12
3	347	1.22E+12
4	289.1	1.11E+12

*1 $RU = 0.1\ ng/cm^2$

Figure 3.12: Zoom on the binding of oligonucleotides with gluataraldehyde (GA) in the case of APTMS coating. Channels are listed as: 1 (red), 2 (green), 3 (blue) and 4 (pink). The buffer solution is 0.01x PBS. The *method* includes: injection of 10% glutaraldehyde (GA) for 30min and 20min injection of 2μM 50A ssDNA in 0.01xPBS.

In **Figure 3.12**, next to the column of RU values there is a column which indicates the correspondence DNA density values. The conversion factor has been extracted by [9], but here it has been expressed in nanograms over cm squared. Its value is therefore equals to 0.1 ng/cm^2.

The same discussion can be carried out for the AUTES samples, and the outcomes are shown in **Figure 3.11** and **Figure 3.13**. A comparison between the two types of coating can be easily carried out by creating histograms with the data collected in the previous tables. **Figure 3.14** and **Figure 3.15** represent the DNA density versus the channel's number, respectively for APTMS and AUTES samples. In the case of APTMS, the

columns from the second sample (S2) of the fourth deposition (DEP4) are the one related to the sensograms showed before. In the histogram, all the different attempts made in this thesis work have been reported. They include changes in DNA concentration, substitution of DNA molecule and use of different buffer solutions.

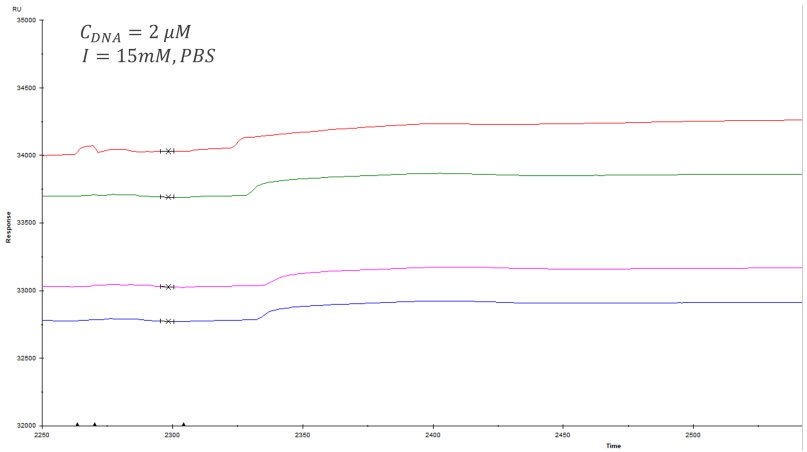

Oligos immobilization:
50A

Channel	RU*	DNA density [DNA/cm2]
1	178.3	6.82E+11
2	62.2	2.38E+11
3	54.6	2.09E+11
4	53.6	2.05E+11

*1 $RU = 0.1\ ng/cm^2$

Figure 3.13: Zoom on the binding of oligonucleotides with gluataraldehyde (GA) in the case of AUTES coating. Channels are listed as: 1 (red), 2 (green), 3 (blue) and 4 (pink). The buffer solution is 0.01X PBS. The buffer solution is 0.01x PBS. The *method* includes: injection of 10% glutaraldehyde (GA) for 30min and 20min injection of 2μM 50A ssDNA in 0.01xPBS.

The first change concerns the DNA concentration: a higher DNA concentration up to 5μM had been tested with respect to the usual 2μM. In principle, a higher DNA concentration should lead to a higher Biacore signal due to the higher probability that biomolecules attach to the surface. However, results show no particular improvement in the RU values. This is also confirmed by the very fast transient present in **Figure 3.11** in correspondence of the oligonucleotides binding, which means that the surface is already saturated at lower DNA concentration. Therefore, in order to save DNA for further experiments, lower DNA concentrations have been favoured.

Before changing other process parameters, during the fourth deposition of APTMS, some practical improvements have been accomplished. Examples of those improvements include:

- Freezing Biacore samples one by one to avoid degradation caused by defrosting.
- Preparing a 500ml stock of 0.1xPBS and storage it in the fridge (4.5°). Picking up the desired amount each time before the experiment, around half an hour before using.
- Rinse Biacore samples with acetone and IPA before using. Always blow with N2 after the rinsing procedure.

By using different experimental and maintenance conditions, some ameliorations in terms of process reliability have been achieved and the results can be observed by looking at the four columns of the fourth deposition process (DEP4) in **Figure 3.14**.

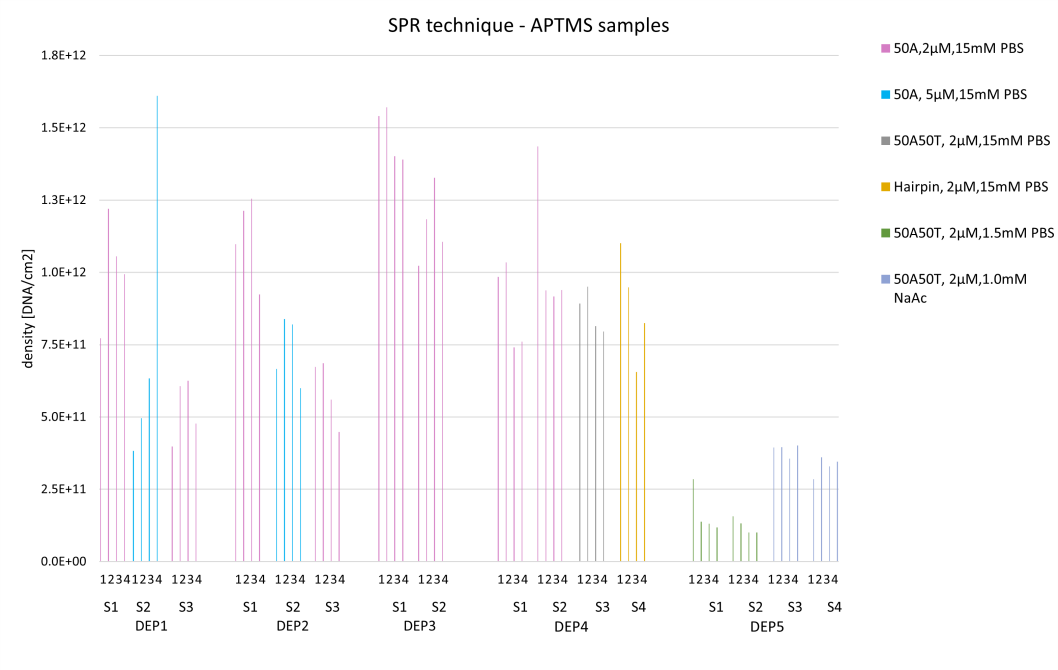

Figure 3.14: Estimated DNA density for various APTMS samples. Different experimental conditions are represented by different column's colours.

The second parameter that has been changed concerns the type of DNA molecule adopted during the binding procedure. The different types of molecules have already been described in detail in Sec. 2.2.5. They differ in length and structure, but mainly in their charge. Each DNA nucleotide carries a charge equal to 1 elementary charge [12]. So, the larger is the number of nucleotides present in the DNA molecule, the higher the total charge becomes. As a consequence, also the bioFET signal should be boosted. However, in the case of SPR measurements we are still dealing with bare oxide samples. Therefore, it is reasonable that almost no differences are visible when different molecules are analyzed. This behavior is shown in **Figure 3.14**, by focusing on the SPR results of the fourth deposition (DEP4).

The last change in the experimental conditions during SPR measurements is the modification of the buffer solution. In particular, buffer solutions with lower salinity have been exploited. First, the same PBS solution has been exploited by simply modifying the dilution. Starting from a 1X stock PBS solution, a 100 times dilution has been performed in order to obtain a 1.5mM PBS solution. This type of buffer is meant to be used at neutral pH values, where the zeta potential curve of APTMS is very steep (see **Figure 3.9**). Therefore, an alternative buffer solution to be tested is sodium acetate (NaAc), which works at lower pH values (around 5). At those pH values, at least in the case of

APTMS coating, the zeta potential curve stabilizes at a constant value. These conditions have been tested during the last deposition process (DEP5). By looking at those columns in **Figure 3.14**, the results obtained from same experimental conditions are stable and reproducible. This aspect confirms that the practical improvements implemented starting from the fourth deposition are actually a good practice to follow.

For what concerns the DNA density values in the case of different buffer solutions, the SPR signal is lower with respect to the previous ones with higher salinity. This effect is predictable because the Debye length within the electrolyte solution becomes higher if the salinity of the buffer solution decreases. As a consequence, less molecules can bind to the surface due to the higher charge screening. However, when dealing with bioFETs, the binding of biomolecules is effective just if there is a net changing in the charge present at the channel's surface. This means that a larger Debye length is actually beneficial for the charge detection in biosensors based on FETs. The trade off in salinity looks like a paradox: in order to have the highest DNA density signal, the buffer salinity must be the highest one. But, doing so it is likely that the resulting bioFET signal will not be the highest possible. Therefore, the strategy used in this work consists in using a lower buffer salinity that will increase the probability to detect target molecules.

Before implementing this strategy on bioFET sensors, it is reasonable to check whether the DNA binding is still possible by using this new condition. By looking at the results in **Figure 3.14**, using sodium acetate as buffer solution seems more promising with respect to the use of 1.5mM PBS solution. However, the maximum DNA surface density detected from SPR measurements never overcomes $5\text{x}10^{11} DNA/cm^2$ ($M_{w,50A50TDNA} = 31198.6 g/mol$, [from datasheed]). This value seems quite low if compared to previous works [24], where the detection limit with a 15mM PBS buffer solution is about $5\text{x}10^{11} DNA/cm^2$. Nevertheless, both the SAM and the tested molecules were different, thus no proper comparisons can be carried out.

For what concerns the AUTES coating, SPR measurements have been performed just in one condition: 2μM 50A DNA oligonucleotides and 15mM PBS buffer solution. No particular investigation has been carried out on AUTES samples because the resulting DNA density is very low. Especially, if compared to the results of APTMS coating performed with the same conditions.

It is important to highlight that the very high SPR signals obtained from channel 1 in **Figure 3.15** has to be attributed to a malfunction of the channel itself, that has been solved lately. Moreover, negative density values are illogical and inconsistent. Therefore, they must be correlated to other unpredictable malfunctions or problems occurred during the experiments.

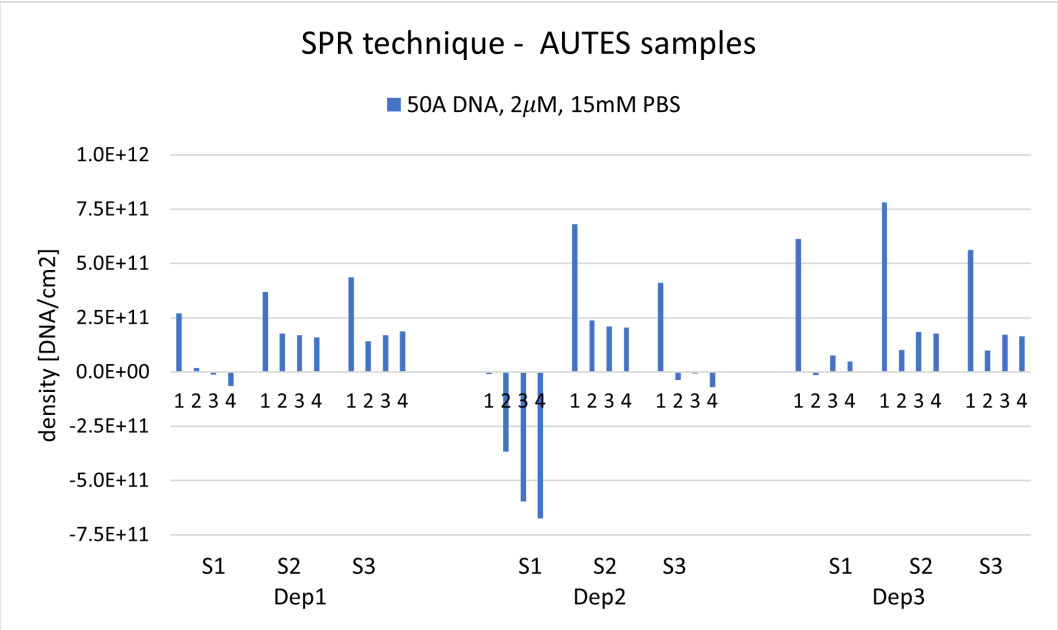

Figure 3.15: Estimated DNA density for different AUTES samples. Negative results have to be interpreted as experimental failures. Experimental condition: 2μ 50 DNA oligonucleotides in a 15mM phosphate-buffered saline (PBS) solution.

3.2 Conclusion

In this chapter, the surface chemical characterization of two types of aminoalkylsilane functional layers has been explored. Among the many surface characterization techniques currently existing, measurements of contact angle (CA), thickness, surface potential, chemistry composition and real-time molecule binding have been performed. The Contact Angle measurements show that the APTMS coating with a CA between 35° and 45° is more hydrophilic compared to the AUTES coating, where the CA is about 80°. Ellipsometry measurements indicates an APTMS coating thickness of around 1.7 nm, while for AUTES the measured thickness is only 0.8 nm. The chemistry composition and more specifically, the amino group content in the functional layer is determined with FTIR measurements. In the case of AUTES, a well-defined peak indicating the presence of amino groups does not arise in the spectrum. In contrast, for the APTMS coating the amino peak is clear and reproducible. Streaming potential measurements do not highlight a large difference between the two coatings: the surface remains quite negatively charged at higher pH in both cases. Eventually, results concerning the binding protocol of DNA oligonucleotides with gluataraldehyde have been presented. The SPR results show a maximum DNA density of $2.5 \cdot 10^{11}$DNA/cm^2 in the case of AUTES, while the density is one order of magnitude higher in the case of APTMS, where the DNA density can reach $1.5 \cdot 10^{12}$ DNA/cm^2. As a conclusion, the higher surface density of bound DNA and the clear amino peak in the FTIR spectrum of the APTMS coating make the APTMS coating the most straightforward choice to test on the bioFET sensors.

Chapter 4

bioFETs characterization

In this chapter, the experimental results concerned the electrical characterization of the bioFETs are shown and discussed. In the first part, the bioFETs are characterized by means of two main parameters: the threshold voltage (V_T) and the subthreshold swing (SS). They are extracted from the $I_{DS} - V_{GS}$ characteristics of the devices present on the bioFET chip and they are compared in order to choose one single selective device per chip. Based on the results, the variation of the I_{DS} in time for the chosen device is monitored during the binding protocol of different biomolecules. In particular, the binding of single-stranded DNA oligonucleotides with the functionalized surface is the goal to be reached.

4.1 I_{DS} -V_{GS} characteristics

The representation of results derived by the electrical characterization of the bioFETs is shown following the experimental work flow. Since a bioFET chip per time has been analyzed during a single experiment, the outcomes reported hereafter are associated to a bioFET chip only. However, the experiment has been repeated other times in order to study the reliability of the method. Similar results have been derived by the experimental analysis of distinct bioFET chips, but only the ones obtained by different experimental conditions have been reported and discussed.

As already mentioned in Sec. 2.5, the first measurement to be performed is the $I_{DS} - V_{GS}$ characteristics of all the devices present on the chip. More than 100 devices are analyzed to check their parameters. An example of the curves obtained after this first process step is reported in **Figure 4.1**. The device under study has the following channel's dimensions: $W_{ch} = 20nm$, $H_{ch} = 30nm$ and $L_{ch} = 90nm$. The good quality of the device can be noticed by looking at the steepness of the curve in the subtreshold region and the almost coincident upsweep and downsweep curves. In particular, the near-ideal subthreshold swing (SS) of $64mV/dec$ and the nearly null hysteresis (ΔV_0) of 7mV confirm the evidence. Therefore, the reported example is one of the 25 devices chosen for the stability study. In principle, also the other ones have similar properties. The main difference is about the device's dimensions, especially for what concerns the gate length. The

different values that it can assume are reported in **Table 4.1**.

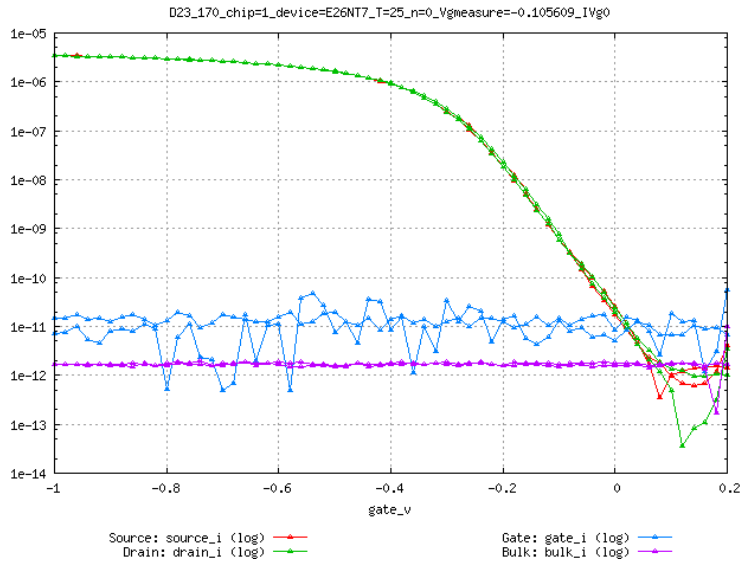

Figure 4.1: $I_{DS} - V_{GS}$ characterization of device E26NT7 with APTMS coating (chip number 170). $V_{DS} = -0.1V$, $-1V \leq V_{GS} \leq 0.2V$. Device's dimensions: W_{ch}xH_{ch}xL_{ch}=20x25x90 nm. Running buffer: 0.1xPBS, pH 7.3. Flow rate: 25μL/min.

Typically, devices with lower gate lengths have been chosen as the selective ones for the electrical characterization. This because the primary goal of the research this thesis work is based on is the single-molecule sensing with silicon bioFETs. Thus, the smaller is the channel length of the device and the higher the probability to detect one target molecule only becomes. Hence, in order to let this thesis work playing a role in the main original goal, priority has been given to devices ExxNT6 and ExxNT7. They have a gate length respectively of 70nm and 90nm. The use of devices ExxNT5 has been avoided because previous studies show that the DNA signal drops for devices with gate length around 50nm [24].

Device	$L_{ch}[nm]$
ExxNT5	45
ExxNT6	70
ExxNT7	90
ExxNT8	130
ExxNT9	250
ExxNT10	1000
ExxNT11	10000

Table 4.1: Different gate lengths of the devices present on the bioFET chip. xx in the device's name represent different possible width values. The height is fixed to 25nm.

After the first stability test, the best device to be analyzed throughout the whole experiment results to be the same one picked up from the scan analysis. The good quality of the device is confirmed by looking at **Figure 4.2**. There, the curves derived by the five consecutive $I_{DS} - V_{GS}$ characterizations are merged. Results show that the curves are always nearly coincident for both the upsweep and downsweep measurements within same repetitions. This evidence confirms an hysteresis almost null for the selective device. In addition, the curves overlap also within different repetitions. The superimposition of distinct $I_{DS} - V_{GS}$ characteristics verifies the reliability of the chosen device in time.
The curves represent only the subthreshold region of the FET, because it is the optimal region to work with in the case of biomolecule sensing [29].

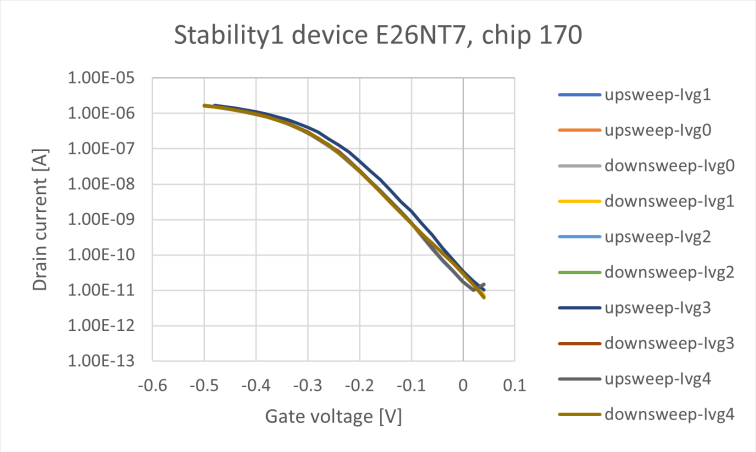

Figure 4.2: $I_{DS} - V_{GS}$ curves of device E26NT7 with APTMS coating (chip number 170) after the first stability study. $V_{DS} = -0.1V$, $0.2V \leq V_{GS} \leq -1V$. Device's dimensions: W_{ch}xH_{ch}xL_{ch}=20x25x90 nm. Running buffer: 0.1xPBS, pH 7.3. Flow rate: 25μL/min.

In order to perform the measurement of the drain current over time, also the gate voltage must be fixed. The drain voltage is already fixed to $V_{DS} = -0.1V$ throughout all the experiment. The criteria for the gate voltage determination is to consider an operating point for the FET where the drain current is within 1nA and 10nA. The lower value of 1nA is chosen for evaluating the threshold voltage shift (ΔV) during the biosensing experiments. It represents a sort of lower limit in order to be sure that the signal is clearly detectable with respect to the background noise. The latter can be related to the gate current that theoretically should be null. In reality, its value is about $10^{-11}A$, as can be seen from **Figure 4.1**. On the other hand, the upper limit of 10nA is chosen based on the results of previous studies. There, the relative drain current signal resulted to be about 400% [24]. Thus, if the baseline is set to 1nA, the DNA signal will increase up to 5nA. By setting the upper limit to 10 nA, it is implicitly said that the expected relative drain current signal will never exceed the 900%.

Table 4.2 reports the values of threshold voltage (V_T), hysteresis (ΔV_0) and subtreshold swing (SS) of the device E26NT7 after the first stability study. Based on those results, the gate voltage is fixed to $V_{GS} = -0.12V$. Doing so, the device can work in the middle of

the subthreshold region and close to the lower limit of 1nA. In particular, with the chosen operating point the initial current is expected to be around 1nA. Afterwards, when (negatively charged) biomolecules bind to the surface of p-type bioFETs, an increase in the drain current is expected due to the extra holes induced in the channel [24]. As already stated before, the final drain current is not supposed to be higher than 10 times the one obtained in the absence of DNA. Therefore, it is relevant to underline that the device will always work in the subthreshold region within all the considered interval.

IVg	$V_0[V]$	$\Delta V_0[mV]$	$V_T[V]$	$SS[mV/dec]$
1	-0.108	0.211	-0.274	66.877
2	-0.107	1.937	-0.274	65.867
3	-0.108	1.960	-0.272	67.501
4	-0.106	0.624	-0.272	64.083
5	-0.107	3.747	-0.275	66.599

Table 4.2: Basic parameters of the $I_{DS} - V_{GS}$ curves extracted from the first stability study on device E26NT7 with APTMS coating (chip number 170) before the molecule binding. The first column refers to measurement's number. In total, the $I_{DS} - V_{GS}$ characterization is repeated five times. V_0 is the gate voltage at constant drain current of 1nA, V_T is the threshold voltage and SS is referring to the subthreshold swing. All of them are the average values between the ones derived from the upsweep and the downsweep measurements. ΔV_0 is the difference between the gate voltage at $I_{DS} = 1nA$ extracted from the upsweep and downsweep curves.

4.1.1 Comparison with bare oxide bioFETs

Until now, only the results derived from the first stability test on APTMS coated bioFETs have been shown. As described in Sec. 2.5, the first stability test is performed before the flushing of glutaraldehyde (GA) in the system. This means that none biomolecules have been attached to the surface till this process step. Thus, it is relevant to show how the APTMS coating affects the main FET parameters extracted from $I_{DS} - V_{GS}$ curves. To this aim, a bare oxide bioFET (a bioFET that did not receive APTMS coating) has been analyzed. For simplicity, only the parameters extracted for the selective device are shown. The results are represented in **Table 4.3**.

The device under test has the same number of the one analyzed before. Its dimensions are W_{ch}xH_{ch}xL_{ch}=20x25x90 nm. The choice of analysing devices with the same dimensions has been intentionally made in order to fairly compare the two devices. In particular, the same device's dimensions guarantee that the APTMS coating is the only factor responsible for the change in subthreshold swing (SS). The parameters extracted from the same device in the two different condition (coating or bare oxide) are compared in **Figure 4.3**. In both cases, hysteresis values have not been represented because their order of magnitude is three times smaller than the relative mean voltage values. Thus, even if the average hysteresis increases of almost 4 times in the case of APTMS bioFETs, its value

IVg	$V_0[V]$	$\Delta V_0[mV]$	$V_T[V]$	$SS[mV/dec]$
1	-0.133	0.579	-0.297	63.034
2	-0.132	0.716	-0.292	63.092
3	-0.135	0.900	-0.292	63.808
4	-0.133	0.429	-0.292	63.063
5	-0.132	-0.077	-0.293	62.715

Table 4.3: Basic parameters of the $I_{DS} - V_{GS}$ curves extracted from the first stability study on device E26NT7 without coating (chip number 176). In total, the $I_{DS} - V_{GS}$ characterization is repeated five times. V_0 is the gate voltage at constant drain current of 1nA, V_T is the threshold voltage and SS is referring to the subthreshold swing. All of them are the average values between the ones derived from the upsweep and the downsweep measurements. ΔV_0 is the difference between the gate voltage at $I_{DS} = 1nA$ extracted from the upsweep and downsweep curves

is still acceptable and negligible.

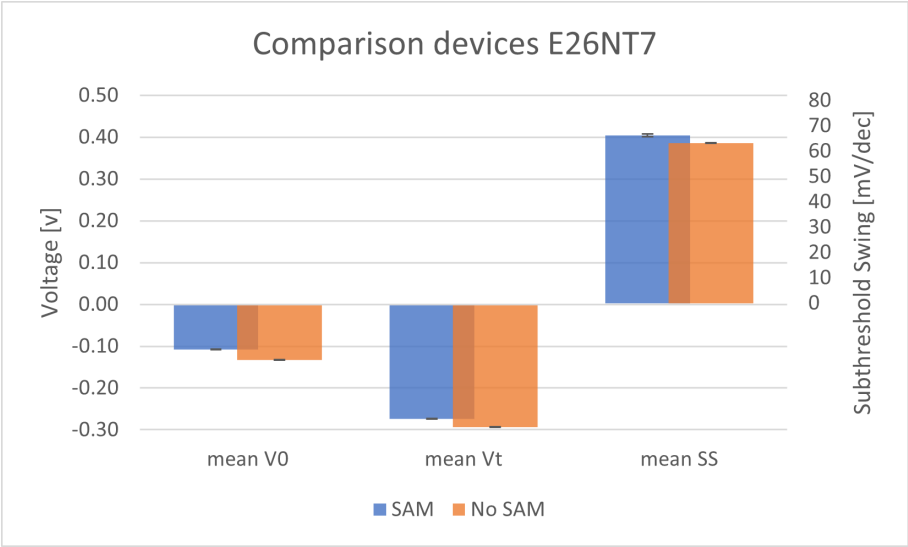

Figure 4.3: Parameters extracted from the first stability study of device E26NT7 with APTMS coating (chip number 170) and without coating (chip number 176). The measures are the averages of the same parameters derived by the five $I_{DS} - V_{GS}$ curves. $V_{DS} = -0.1V$, -1V$\leq V_{GS} \leq$ 0.2V. Device's dimensions: W_{ch}xH_{ch}xL_{ch}=20x25x90 nm. Running buffer: 15mM PBS (pH 7.3) for SAM sample, 0.1mM DIW+HCl (pH 4) for bare oxide sample. Flow rate: 25μL/min.

The results derived from the comparison of the same device with or without the SAM coating show promising outcomes for the APTMS functional layer. The bioFETs with SAM are merely effected by the presence of APTMS molecules on the surface. The voltage at a constant drain current of 1nA (V_0) is just few tens of mV smaller with respect to the bare oxide one. It means that the $I_{DS} - V_{GS}$ curve relative to the SAM-coated

sample is shifted towards smaller gate voltages. In principle, it is a good factor because smaller gate voltages are needed to reach the same working point (I_{DS}=1nA).

For what concerns the threshold voltage (V_T), a comparison in terms of absolute value is not suitably possible because the buffer solutions used during the two experiments are different. In particular, what affects the threshold voltage is the pH value of the liquid injected through the flow cell. Nevertheless, in both cases the resulting value is around $V_T = -0.3V$. This value is consistent with a common criteria in CMOS circuits which states that the on-current should be at least 100 times the off-current at $V_{GS} = V_T$. In this case, the former is derived by the experiment and it is equal to $\sim 10^{-7}A$. The latter is represented by the gate current and it is around $10^{-11}A$. Therefore, the criteria is fulfilled because the ratio is $\sim 10^4$ and the resulted threshold voltage can be considered reasonable.

The other important parameter is the subthreshold swing (SS) value. In the case of bare oxide it is around $63mV/dec$, while it increases up to $66mV/dec$ when the SAM is deposited on the surface. Theoretically, in inversion mode devices the gate capacitance is almost equal to the oxide one. Moreover, it does not depend on external voltages because the oxide capacitance depends only on technology ($C_{OX} = \epsilon_{OX}/t_{OX}$). The presence of further molecules on top of the FET channel is supposed to reduce the capacitance value. The reduction of the gate capacitance leads to the increase of the bulk charge linearization coefficient, also called slope factor (m). It assumes the unitary value just in the case of infinite oxide capacitance. Therefore, if the oxide capacitance is decreased by the presence of the SAM, the slope factor will be higher. By considering the definition of the subthreshold swing (SS):

$$SS = 2.3 \cdot m \cdot \frac{k_B T}{q} \tag{4.1}$$

by increasing the slope factor (m), also the subthreshold swing (SS) will go up. As a consequence, the device's performances will be affected negatively. The results of **Figure 4.3** confirm this analysis because of the increasing trend in the subthreshold swing. However, the increment of subthreshold swing (SS) due to the presence of APTMS coating exceeds of just $3mV/dec$ the initial one, which is already close to the ideal value($\sim 60mV/dec$). This result denotes the good quality of the device even considering the additional functional layer on the top. Moreover, it is relevant to underline that the result is much better than the one obtained with other types of SAM deposited on the same devices. In previous works [24], an azide $C_{11}N_3$-SAM was deposited on the bioFETs, showing a subthreshold swing of about $\sim 80mV/dec$. The resulting higher value of subthreshold swing has been explained due to the high density of the $C_{11}N_3$-SAM layer (98% surface covarage) [16]. Thus, following the same reasoning, the smaller subthreshold swing in the case of APTMS coating can be justified by the smaller density of the functional layer. This characteristic is also confirmed by the moderate peaks obtained in the FTIR spectra during the chemical characterization. As a result, a great improvement in terms of electrostatic channel control is reached thanks to the use of APTMS coating on bioFETs.

4.2 Biomolecule sensing

The first molecule to be injected in the fluidic system is glutaraldehyde (GA). The protocol for GA molecule consists in 30 min of GA injection followed by 15 min injection of 0.1X PBS buffer solution. Gluataraldehdye concentration is 25% (in DIW), taken directly from the provider's bottle (Sigma-Aldrich). **Figure 4.4** represents the result of the GA timetrace. The formyl groups (CHO) of GA are supposed to bind to the amino groups (NH2) on the surface of the bioFETs. As a consequence, a different surface charge results on the channel's surface, leading to a different amount of current. The new baseline can be seen at the end of the timetrace, after the switching to the buffer solution (0.1xPBS, pH 7.3).

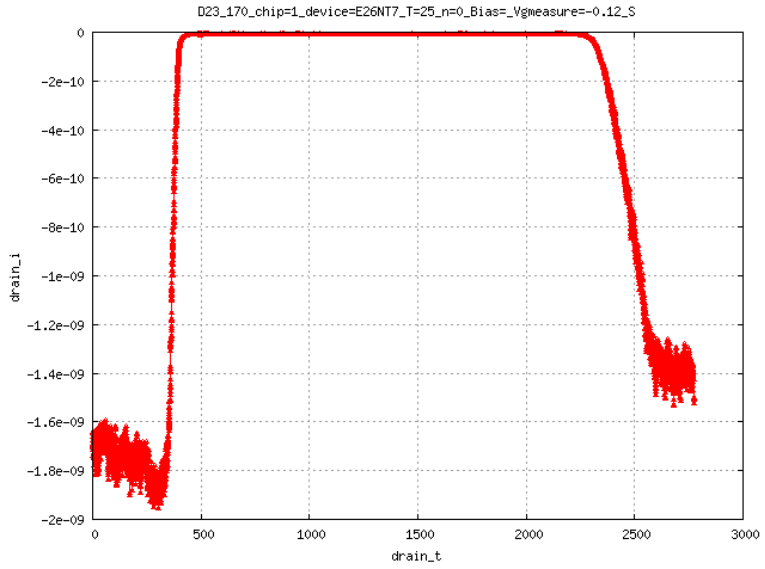

Figure 4.4: $I(t)$ curve of device E26NT7 with APTMS coating (chip number 170) during the injection of glutaraldehyde (GA) in the flow cell. $V_{DS} = -0.1V$, $V_{GS} = -0.12V$. Device's dimensions: W_{ch}xH_{ch}xL_{ch}=20x25x90 nm. Running buffer: 15mM PBS, pH 7.3. Flow rate: 25μL/min. Protocol: 30 min GA + 15 min 0.1xPBS.

Before performing the DNA binding, another timetrace is performed by injecting the buffer solution only (0.1xPBS, pH 7.3). The sample under test is called dummy and the corresponding result is represented by the blue curve in **Figure 4.5**. This step is necessary because the injection of different solutions in terms of ionic strength and pH value can change the baseline. Thus, it is important to have a reliable current reference before injecting the target molecules.

Next, the chosen DNA oligonucleotides are injected. In this experiment, a sequence of 50A50T with a concentration of 2μM is used. The DNA is suspended in the same solution exploited as running buffer (0.1xPBS). Thus, the immobilization buffer coincides with the running buffer, so as differences in the drain current may be attributed to the biomolecule only.

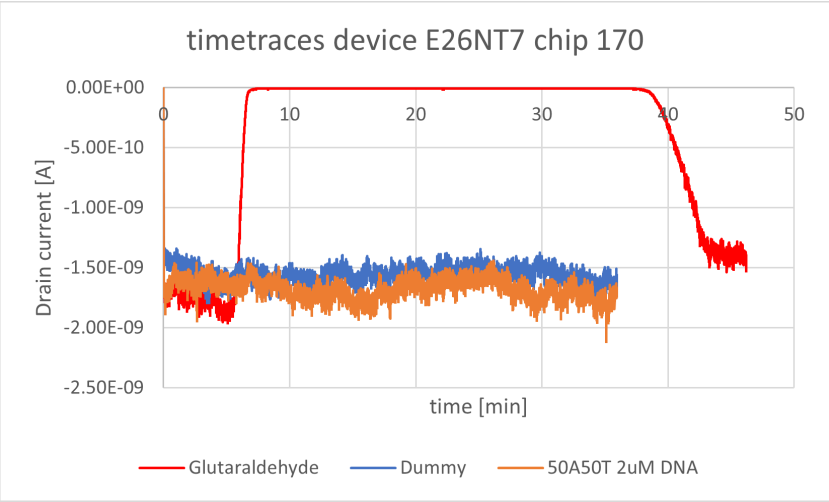

Figure 4.5: Comparison between $I(t)$ curves of device E26NT7 with APTMS coating (chip number 170) during the injection of different fluids. $V_{DS} = -0.1V$, $V_{GS} = -0.12V$. Device's dimensions: W_{ch}xH_{ch}xL_{ch}=20x25x90 nm. Running buffer: 0.1xPBS, pH 7.3. Flow rate: 25μL/min. DNA molecule: 2μM 50A50T Oligonculeotides. Protocol for DNA binding: 20 min DNA + 15 min 0.1xPBS.

The orange curve in **Figure 4.5** represents the outcome after the flushing of DNA. The signal obtained from the timetrace analysis of DNA binding is nearly coincident with the dummy one. It is always around $I_{DS} = -1.5nA$. The outcome does not provide the evidence of any additive molecules bound to the surface, at least in the nearby of the channel. The reasons why no DNA signal has been detected during the experiment may be many. The first one concerns the intrinsic structure of the bioFETs, which is based on the presence of a cavity between source and drain interconnections. The channel region is intrinsically determined by the cavity itself. This feature was completely missing in the samples analyzed during the chemical characterization, which were flat bare oxide Si dies. Therefore, a reasonable amount of uncertainty about the presence of biomolecules on the bottom of the cavity may arise. Nevertheless, the different baseline that appears after the glutaraldehyde (GA) injection seems to demonstrate the presence of the chemistry which GA binds to.

The second hypothesis concerns the characteristic length for the extension of the electrical double layer (EDL) within the APTMS coating. By definition, the expression of the Debye length is:

$$\lambda_D = \sqrt{\frac{\epsilon\epsilon_0 k_B T}{2q^2 I}} \tag{4.2}$$

where ϵ is the permittivity of the fluid, ϵ_0 is the vacuum permettivity and I is the ionic strength of the solution. In the case of 0.1xPBS buffer solution, the salinity is equal to 15mM and the Debye length (λ_D) results to be around 2.5nm. By doing trivial calculations, the total approximate molecule length of glutaraldehyde (l_{GA}) is around 0.6nm.

From the literature, the DNA width is around 2nm [13]. Specifically, we are interested in the width and not in the length of the DNA because the ssDNA is considered to lie horizontally on the sensor's surface. This is due to the chosen type of amino-modified oligonucleotides, where both extremities are activated with NH2 groups. From the surface characterization results, the APTMS layer has a thickness around 1.8nm (Sec. 3.1.2). By summing up all the terms, the DNA distance from the surface results to be between 2.4nm and 4.4nm. Since DNA has a certain elasticity, the real DNA distance will depend on the binding site of DNA with the molecules at the surface. The total thickness of the functional layer results to be larger than the Debye length, when adopting a 15mM PBS buffer solution. By considering the theory expressed in Sec. 1.1.4, the signal rapidly decreases with an exponential trend after the Debye length. Thus, it is possible that the DNA molecules bind, but the signal is too low to be detected.

Naturally, the total thickness of the overall SAM cannot be changed arbitrary. Therefore, the only way to change this parameter would be to choose either a different chemistry or binding protocol. For this reason, the strategy adopted in this thesis work is to increase the Debye length instead of decreasing the SAM thickness. The goal is achieved by testing another experimental condition. It consists in using a new buffer solution characterized by a lower ionic strength. In particular, a sodium acetate buffer solution (NaAc) with pH 4.9 and ionic strength equals to 1.0mM has been selected. The correspondence Debye length becomes around 10nm, which is bigger than the upper limit imposed by analyzed structure. The resulting timetraces obtained with this new experimental condition are reported in **Figure 4.6**.

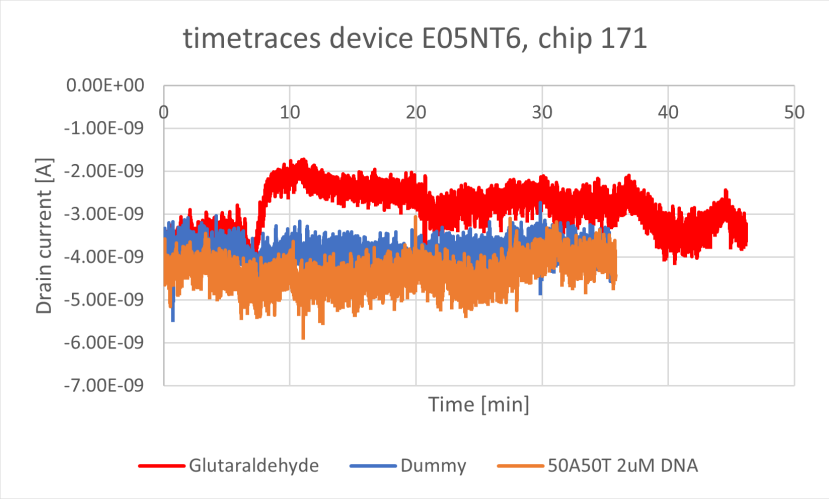

Figure 4.6: Comparison between $I(t)$ curves of device E05NT6 with APTMS coating (chip number 171) during the injection of different fluids. $V_{DS} = -0.1V$, $V_{GS} = -0.28V$. Device's dimensions: W_{ch}xH_{ch}xL_{ch}=15x25x70 nm. Running buffer: 1.0mM NaAc, pH 4.9. Flow rate: 25μL/min. DNA molecule: 2μM 50A50T oligonculeotides. Protocol for DNA binding: 20 min DNA + 15 min 0.1xPBS.

By looking at the results of the experiment, no relevant differences can be noticed with respect to the previous experimental condition. The DNA signal is still nearly coincident with the dummy one along all the timeline. The absolute value of the current increases with respect to the previous case just because the devices are biased with a more negative gate voltage. This is consistent with the use of p-type devices, where the drain current increases for negative gate bias. The reason why the DNA signal is still not present may be attributed to the lower density of DNA molecules at the surface. Indeed, results of Biacore experiments (Sec. 3.1.5) showed a SPR signal that is one order of magnitude lower with respect to the one derived by using 15mM PBS as buffer solution. It is evident that a trade-off between larger Debye length and decent charge screening is needed to obtain a reasonable DNA signal.

4.3 Conclusion

In this chapter, the good quality of the silicon FETs used for the biomolecule sensing has been demonstrated. In particular, two main parameters of the $I_{DS}-V_{GS}$ curves have been considered in this study: the threshold voltage (V_T) and the subthreshold swing (SS). Both parameters have been analyzed for bare oxide bioFETs and for bioFETs coated with APTMS. The threshold voltage of the devices under test is around $V_T = -0.3V$, that is a good value for nano sized bioFETs because it allows to exploit low gate voltages to turn the devices on. The difference in threshold voltage between coated and uncoated bioFETs can be related to the different pH of the buffer solutions used during the two experiments, which intrinsically affects the V_T value. The subthreshold swing (SS) for APTMS coated bioFETs is around $66mV/dec$ close to the SS of state-of-the-art micron length ISFETs ($\sim 60mV/dec$). In contrast with the threshold voltage, the subthreshold swing can be compared between the two experiments because it does not depend on the buffer solution. Its value is only a few mV/dec larger compared to the SS of the bare oxide bioFETs, which is around $63mV/dec$. This result is very promising with respect to previous attempts with different coatings.
Later, the real-time drain current has been reported for two kinds of experiments. For both experiments, 2μM 50A50T DNA oligonucleotides are injected after the activation of the surface with glutaraldehyde (GA). Only the measurement buffer differs between both experiments. First, a diluted phosphate buffer saline (PBS) solution with salinity $I = 15mM$ has been used. For this ionic strength, the predicted Debye length λ_D is about 2.5nm. The second measurement buffer is a sodium acetate (NaAc) solution with $I = 1.0mM$. The estimated Debye length is around 9.6nm. The larger Debye length for the NaAc solution in the second experiment should result in a higher DNA signal. In practice, the experimental results do not show a clear difference in the real-time drain current signal. The lower density of DNA molecules at the surface and the consequent decrease in charge screening could be the cause of the resulting signal, but further experimental evidence could not be obtained because of the lack of time to perform additional experiments.

Chapter 5

Conclusions and outlook

5.1 Conclusions

Nowadays, biomolecule sensing has become a well-known topic in the electronics field because of the increasingly use of micro and nanotechnologies for the development of more sensitive and specific biological sensors. Various biosensing strategies have been investigated during decades [22], but a large-scale single-molecule sensing platform competitive with the usual optical ones has still to be accomplished. A similar electronic platform could further increase the sensor density (from 8 million to a billion [24]) thanks to the lower costs and higher throughput derived by the use of top-down photolithographic processes. Indeed, the top-down techniques massively used in the electronics industry are intrinsically characterized by high yields and uniformity. Consequently, this realization could open doors for breakthroughs in high-end applications like sequencing and DNA storage.

In this work, we focus on a liquid-gated bioFET sensor based on molecule detection by means of the field-effect. Its fabrication is very similar to the one implemented in standard CMOS technology characterized by more than 1 billion transistors in a single chip. Therefore, also the sensor scalability of our bioFETs is thought to be in the same range. In this thesis, we investigate the possibility to develop a surface coating for bioFET chips with low surface charge and low pH sensitivity, while still maintaining a functional bioFET sensor. The expected boost in bioFET sensitivity due to surface engineering could be a key factor to enable single-molecule detection with silicon-based bioFETs. However, the final binding protocol for amino-modified single-stranded DNA oligonucleotides with the new developed coatings does not seem to produce positive results. In this work, these issues are tackled by performing different experimental conditions. Other feasible attempts for the successful detection of DNA are just listed in this chapter. Indeed, further experimental evidence could not be obtained because of the lack of time to perform additional experiments.

The complete methodology of the experiments performed during this thesis work is described in Chapter. 2. Based on those protocols, the development and characterization

of two types of aminoalkylsilane functional layers have been carried out in Chapter 3. 3-Aminopropyltrimethoxysilane (APTMS) and 11-aminoundecyltriethoxysilane (AUTES) chemistries have been analyzed as possible surface coatings for bioFET chips. First, as a reference, the surface of bare silicon dioxide samples has been characterized. Afterward, surface characterization on both APTMS and AUTES coated samples has been performed. Measurements of contact angle (CA), thickness, surface potential, chemistry composition and real-time molecule binding have been performed.

The APTMS coating results to be the best one because of the resulting higher hydrophilicity of the surface. Its CA is between 35° and 45°, while it reaches 80° in the case of AUTES coating. Surface wettability is an important factor when dealing with nano-scale cavity filled with liquids, where capillary effect and surface tension are more relevant. Another advantage of APTMS coating is the lower surface charge at neutral pH, deducible from the smaller zeta potential (in absolute value) obtained during surface potential measurements. On the other hand, ellipsometry measurements reveal that APTMS coating is not a proper self-assembled monolayer (SAM) because its thickness is always around 1.7nm. This value is almost three times the thickness of a single APTMS layer [1]. This mean that APTMS chemistry polimerizes during the vapor-phase deposition process to form multi layers.

However, the very thin layer formed by AUTES chemistry (thickness$\sim$0.8nm) is not so efficient. This is confirmed by FTIR measurements on AUTES samples, which indicate the lack of a well-defined peak in correspondence of the amino absorbance range. This result discloses possible binding issues with further biomolecules sent in proximity of the surface. The problem concerns the terminal groups of the AUTES layer, which remain hidden from the top of the surface. Eventually, this condition will prevent the binding of the target molecules to the surface. This hypothesis is confirmed by SPR measurements, where a binding protocol for amino-modified single-stranded DNA oligonucleotides is established and carried out. In principle, we expect that the amino terminal groups (NH2) of the functional layer bind to the first formyl groups (CHO) of GA. Then, the other formyl group of GA bind to the amino-modified ssDNA oligonucleotides, leading to the detection of the target molecule. SPR results show a maximum DNA density of $2.5\text{x}10^{11} DNA/cm^2$ in the case of AUTES. This is quite a low value, if compared to previous works on the same topic [24].

In the case of APTMS coating, the same kinds of measurements provide a maximum DNA density of $1.5\text{x}10^{12} DNA/cm^2$, that is one order of magnitude higher than the AUTES one. Hence, the APTMS coating is the most straightforward choice to test on bioFET sensors, because it guarantees a higher DNA surface density after the binding protocol. Moreover, the APTMS coating exhibits higher hydrophilicity of the surface, together with a lower surface charge, which is shown to significantly enhance the bioFET signal [19].

In Chapter 4, the binding protocol already tested during SPR measurements is repeated

by performing the electrical characterizations of bioFET chips coated with APTMS. The electrical measurements of bioFETs are carried out using a pressure-driven fluidic setup. Measurements are performed on a Probe station equipped with 4 source-measure units (SMUs) to control all the relevant quantities of the system. They are the source-to-gate voltage (V_{GS}), the source-to-drain voltage (V_{DS}), the drain (I_{DS}) and the gate current (I_{GS}). Based on the resulted $I_{DS} - V_{GS}$ curves, the devices are characterized in terms of two important electrical parameters like threshold voltage (V_T) and subthreshold swing (SS).

First, we show the good quality of the used bioFET devices down to a gate length of 70nm and width equal to 15nm, with and without the coating. For what concerns the threshold voltage, in both cases it is around $V_T = -0.3V$ and it is a good value for nano-scale p-type bioFETs because it allows to use low gate voltages as operating point. On the other hand, the subthreshold swing (SS) for APTMS coated bioFETs is around $66mV/dec$ and it is close to the SS of state-of-the-art micron length ISFETs ($\sim 60mV/dec$). Since its value is almost independent from the experimental condition, we can also compare it with the SS of the bare oxide bioFETs, which is around $63mV/dec$. The value of SS obtained for APTMS coated bioFETs equal to $66mV/dec$ is very promising with respect to previous attempts with different coatings. In particular, studies on azide $C_{11}N_3$-SAM deposited on the same type of bioFETs report SS$\sim$ $80mV/dec$. As a consequence, we experimentally demonstrate a great improvement in terms of electrostatic channel control thanks to the use of APTMS coating on our bioFET sensors.

Next, a binding protocol for the detection of 2μM 50A50T DNA oligonucleotides has been implemented on APTMS coated bioFET chips, after the activation of the surface with glutaraldehyde (GA). First, a diluted phosphate buffer saline (PBS) solution with salinity $I = 15mM$ has been used. Then, a diluted sodium acetate (NaAc) solution with $I = 1.0mM$ is adopted. The predicted Debye length (λ_D) increases respectively from 2.5nm to 9.6nm, rising the probability to obtain an higher signal from the presence of DNA molecules. However, no experimental evidence for an improvement in the DNA signal is shown by our measurements. This result may be due to the lower charge screening at the surface that decreases the amount of DNA molecules binding to the glutaraldehyde. Another hypothesis could be the presence of unexpected molecules at the top of the surface, that are different from the amino terminal groups. This condition may generate additive chemical reactions, that hinder the forecast binding process. Examples of these unwanted terminal groups could be residual silanols groups or carbon atoms deriving from APTMS and GA chemistries.

5.2 Outlook

The presented thesis work has been focused on the development and characterization of two types of aminoalkylsilane functional layers for our bioFET sensors. However, not all the types of characterization techniques have been analyzed during the brief period in which this thesis has been conducted. Therefore, a good idea would be to exploit

atomic force microscope (AFM) measurements to check the morphology of the surface. Perhaps, by analyzing the surface of the bare oxide bioFETs first. Then, by performing the same measurements on the bioFETs coated with APTMS. After considering the types of molecules actually present on the surface, we may have a better idea about the binding protocol to be used. Moreover, we could check the validity of the last assumption made in the previous section.

Another possible experiment to be performed is the electrical characterization of bioFET sensors coated with AUTES. This further attempt could validate the hypothesis for which the high thickness of the APTMS layer prevents the successful biomolecule sensing. In particular, the exploitation of a thinner functional layer like the AUTES one will allow for the use of buffer solutions with higher salinity. For instance, the phosphate buffer saline (PBS) solution with salinity $I = 15mM$. In this case, the lower Debye length generated by using a buffer solution with higher salinity would be compensated by the lower thickness of the AUTES coating. Which eventually should generate a decent charge screening effect. Furthermore, by carrying out this analysis on bioFETs coated with AUTES we could better understand whether the two assumptions made in Sec. 5.1 are correlated or not.

Once these issues have been solved, the idea is to use this real-time measurement to proceed towards the electrical verification of single-molecule detection with our nano-scale silicon-based bioFETs. In particular, the goal is to demonstrate that our aminoalkylsilane functional layer is more efficient than the azide $C_{11}N_3$-SAM previously analyzed on our bioFETs. To this aim, by performing the electrical characterization of bioFET sensors in the case of 2μM DNA and 1.5mM PBS solution, we would expect to obtain a relative drain current signal higher than 400% [24]. Equivalently, in terms of threshold voltage shift, we would expect a voltage difference larger than 40 mV to obtain an amelioration with respect to the previous study.

However, an intrinsic limitation of our bioFET sensors is to be all area modified (AAM) devices, which means that biomolecules are immobilized on the entire surface of the chip [21]. As a consequence, the sensitivity of the biosensor is intrinsically reduced because the molecule signal may arise also from binding sites far from the active area. More generally, statistically speaking there will be always some molecules binding in the large -not active- area of the chip. Those molecules do not contribute to the real DNA signal, therefore their resulting signal could be labeled as a further noise source of the bioFET sensor. For this reason, since the noise signal is never zero in AAM devices, the realization of a single-molecule detection limit is difficult to achieve in similar devices. Hence, in order to obtain biosensors with high signal-to-noise ratio (SNR), the solution could be to use selective surface modification (SSM) devices. It means that the molecules forming the self-assembled monolayer (SAM) modify only the active surface of the device, without contaminating the surrounding substrate [21]. Nevertheless, the surface modification techniques useful to reach this goal are intrinsically high-end and time-consuming. These properties are opposite with respect to the original aim of our bioFET sensors,

that is to obtain high-throughput large-scale single-molecule sensing platforms. Therefore, a trade-off between surface selectivity and sensor sensitivity is needed to be achieved in the design of bioFET sensors. The final goal must be always to boost the molecule signal and to obtain the highest SNR, while still maintaining high-volume requirements for applications with good yield and reliability.

Appendix

A Further results about Zeta Potential Measurements

In this section, we report further outcomes about surface potential meeasurements. The results of different deposition processes have been put together in the same graph. The procedure is repeated for both APTMS and AUTES coatings. The final results are represented in **Figure A.1**.

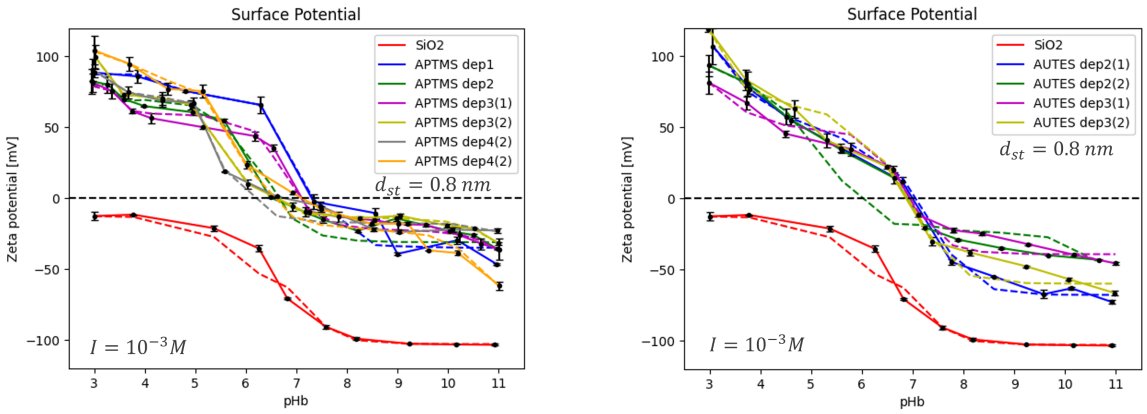

(a) APTMS

(b) AUTES

Figure A.1: Surface potential results. (1) and (2) refer to different samples within the same deposition process. I indicates the ionic strength of the solution used during the experiments. d_{st} is the thickness of the Stern Layer used for the fitting in the *Python* simulation. The value has been extrapolated based on [28], considering *I=1mM*.

As already stated in Chapter 3, surface potential measurements reveal that APTMS coating is more stable at both low and high pH values, where its zeta potential stabilizes with a flat trend. In those regions, a possible pH variation in the nearby of the active area of the sensor does not affect the resulting zeta potential. As a consequence, the molecule binding could be less affected by possibly pH variation. As a general rule, when dealing with biosensors it is better to work in such region. Furthermore, it is known that a neutral or slightly positive surface charge may increase the FET sensitivity [19].

Based on these assumptions, **Figure A.1** shows that the APTMS coating owns a surface

charge that is close to be neutral in a pH range characterized by a flat trend. Moreover, such behavior is exhibited for different repetitions, with good reliability. On the other hand, AUTES coating shows inconsistent surface charges at high pH values and within different repetitions. In addition, the behavior does not improve at low pH values, where the zeta potential is never flat. To sum up, also these further experimental results confirm that APTMS coating is better with respect to AUTES one in terms of surface charge and pH dependence, when working with bioFET sensors.

B Stern parameters in Gouy-Chapman-Stern fitting model

To conclude the part related to surface potential characterization technique, the values of dielectric constant and capacitance attributed to the Stern Layer formed at the interface between each SAM and the electrolyte solution are reported in **Figure A.2**. It is relevant to highlight that such information have not been used in this thesis, because none analytical study has been carried out during this work. Nevertheless, those parameters are easily deducible from the Gouy-Chapman-Stern fitting model used for the interpolation of surface potential measurements in *Python*. Therefore, their values ar reported here for whatever future work on the same topic.

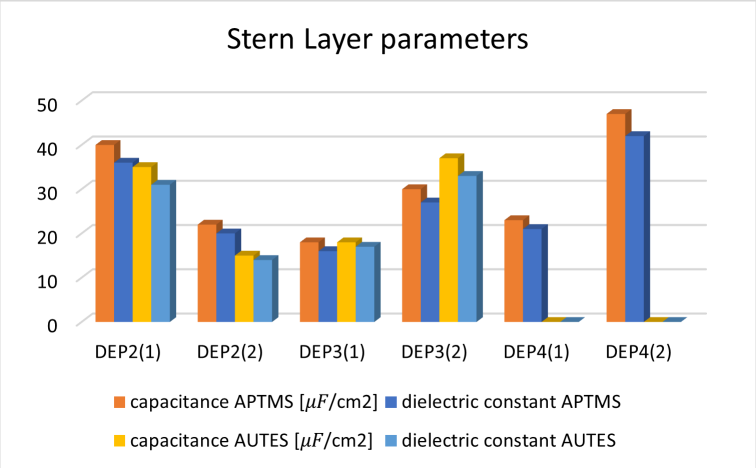

Figure A.2: Stern Layer Parameters for APTMS and AUTES coating. DEP4(1) and DEP4(2) for AUTES are not reported because the fourth deposition of AUTES has never been performed.

Acknowledgements

This master thesis project has been conducted at Imec in Leuven, Belgium. Therefore, it would have been impossible to realize it without the help of Dr. Sybren Santermans, who gave me the opportunity to join the research team. He kindly mentored me in the biosensor field thanks to his background and research experience in single-molecule sensing with silicon bioFETs. Thanks also to Rita Vos and Rabea Hanifa, who patiently guided me in the labs during my internship. Thanks to Prof. Carlo Ricciardi who was the first one to introduce me to sensor science in his course "Physics of NanoBiosystems" during the first year of this master degree. By attending that course, I was really able to find out how passionate I am about bio-science. While, the Imec experience made me realize how fascinating and stimulating is to put into practice my knowledge about nanotechnologies in the research field. I think their combination was the perfect mix for my professional and personal growth. So, thank you both, sincerely.

During the last two years, I have been living far from my home town for the first time of my life. Leaving my family and my close friends to study in another city was difficult, especially at the beginning when I did not know anyone in Turin. However, life made me a gift and in Turin I met three beautiful people who enlightened my daily-life at Politecnico. Thanks to Chiara, Giovanni and Natalia, who have been my guiding lights during the hardest semesters of my life. Natalia, you let me realize how strong a woman can be in this world, once she goes beyond fear. Giovanni, you have been my *semper fidelis* colleague, who fought daily with me to try keeping up with the tough lifestyle of a nanotechnology student at Politecnico. Eventually, my deepest gratitude is expressed to my soulmate Chiara, who is maybe the biggest gift of the last two years. You entered in my life as a hurricane, but differently from it you saved my life. I will never thank you enough. Remember that the red thread of fate that joins us is unbreakable and it will always bring us together again, wherever we could be.

When I thought life had already given to me all the best, I moved to Leuven. In that magical place, I met some of the most wonderful human beings in the world: Sara, Victor, Francesco, Mattia, Erika, Simone and Francesco. Your presence has been fundamental during the last six months. Not only you have filled my working days in Imec and my nights in Oude Markt with fun and joy, but you have also enriched my life with your precious existence. I am so grateful to have known each one of you, and "to have lived the dream" together. I will never forget about you and this amazing experience, which has been the best one of my life. From the depths of my heart: thank you for existing.

If leaving my hometown was difficult, leaving Belgium was heartbreaking. Therefore, thinking about what was waiting for me in Italy had to be stronger than what I left behind me. Luckily, my long-standing friends Elisa, Melissa, Francesca, Margherita, Elisa and Matteo, together with my skating team Genesis and my lovely friend Natasha were there to welcome me back. What I like of our friendship the most is that we will always find each other again, especially in Livorno, which is our special place in the world. No matter how far we could go. Thanks to each one of you to let me feeling always at home again, no matter how long I could stay away. You are my safe place.

Finally, maybe the biggest thanks go to my parents, who gave me the opportunity to fly abroad even if it meant to be far from them. Growing up means also finding your own way in this world, and I can definitely say that going to Turin first and then to Leuven was necessary to find my own way. Those experiences were part of my dreams, and now I can finally say that I realized both of them. Making your dreams come true is a privilege in this world, and my fortune was to have you as parents who gave me the chance to realize them. Without your precious support, it would never have been possible. I know it was hard for you to let me go, but I really appreciated your effort in doing so. As I told you, even if I could stay far from home for a while, I will always come back to you, to take a dive into the sea and to breathe the unique air of Livorno. You are my certainty. I love you now and I will love you forever.

Giada

Ringraziamenti

Questo progetto di tesi magistrale è stato svolto ad Imec, azienda internazionale di ricerca e sviluppo con sede a Leuven, Belgio. Per questo motivo, senza l'aiuto del Dott. Sybren Santermans che mi ha dato la possibilità di unirmi ad un gruppo di ricerca in questa azienda, questo lavoro di tesi non sarebbe esistito. Sybren mi ha guidato con premura nel mondo dei biosensori grazie alla sua conoscenza e alla sua esperienza nel campo della ricerca sulla rilevazione di singole molecole con bioFETs al silicio. Grazie anche a Rita Vos e Rabea Hanifa per avermi guidato pazientemente nei laboratori durante il mio tirocinio. L'altro importante ringraziamento va al Prof. Carlo Ricciardi che per primo mi ha introdotto al mondo sensoristico grazie al suo corso intitolato "Fisica dei nanobiosensori", svolto durante il primo anno di questa magistrale. È proprio grazie a quel corso che sono riuscita a scoprire quanto in realtà fossi appassionata al mondo delle bioscienze. Al tempo stesso, grazie all'esperienza vissuta ad Imec ho potuto capire quanto sia affascinante e stimolante mettere in pratica le mie conoscenze riguardo alle nanotecnologie, coltivando sempre di più la convinzione di voler lavorare nel campo della ricerca. Sono sicura che entrambe le esperienze abbiano contribuito alla mia crescita professionale e personale, e per questo ringrazio entrambi sinceramente.

Negli ultimi due anni, per la prima volta nella mia vita mi sono ritrovata a vivere lontano da casa per molto tempo. Lasciare la mia famiglia e i miei amici più stretti per studiare in un'altra città è stato difficile, specialmente all'inizio quando a Torino non conoscevo nessuno. Tuttavia, è proprio a Torino che la vita ha deciso di farmi un regalo, facendomi conoscere tre persone fantastiche che hanno illuminato le mie giornate al Politecnico. Il mio grazie va a Chiara, Giovanni e Natalia che sono stati i miei punti di riferimento durante i semestri più duri della mia vita. Natalia, tu mi hai fatto capire quanto forte possa essere una donna in questo mondo, una volta che supera la paura. Giovanni, tu sei stato un compagno fedele che ha combattuto con me quotidianamente per affrontare la dura vita di uno studente di nanotecnologie. Infine, grazie alla mia anima gemella Chiara, che è stata forse il regalo più bello degli ultimi due anni. Sei entrata nella mia vita come un uragano, ma a differenza sua, tu mi hai salvato la vita. Non ti ringrazierò mai abbastanza. Ricorda che il filo rosso che ci unisce è indistruttibile e ci riunirà sempre, indipendentemente da dove potremo essere.

Quando pensavo che la vita mi avesse dato già tutto il meglio che potessi desiderare, ecco che mi sono trasferita a Leuven. In quel posto magico ho conosciuto alcuni degli essere umani più straordinari al mondo: Sara, Victor, Francesco, Mattia, Erika, Simone

e Francesco. La vostra presenza è stata fondamentale negli ultimi sei mesi. Non solo perchè avete riempito le mie giornate lavorative ad Imec e le mie serate a Oude Markt con gioia e divertimento, ma anche perchè avete arricchito la mia vita con la vostra preziosa esistenza. Sono molto grata di aver conosciuto ognuno di voi, e di aver "vissuto il sogno" insieme. Non mi dimenticherò mai di voi e di questa fantastica esperienza, che è stata la più bella della mia vita. Dal profondo del mio cuore: grazie di esistere.

Se lasciare casa è stato difficile, lasciare il Belgio è stato straziante. Per questo, pensare a cosa mi stesse aspettando in Italia, piuttosto che a cosa mi stavo lasciando alle spalle è stato fondamentale. Fortunatamente, ad aspettarmi ho trovato i miei amici di una vita: Elisa, Melissa, Francesca, Margherita, Elisa e Matteo, insieme alla mia seconda famiglia Genesis e alla mia dolce amica Natasha. La bellezza della nostra amicizia sta proprio qui: non importa quanto lontano possiamo andare, noi saremo sempre pronti a ritrovarci insieme. Specialmente a Livorno, il nostro luogo del cuore. Grazie a ciascuno di voi per farmi sentire sempre a casa, non importa quanto tempo io stia lontana. Siete il mio posto sicuro.

Infine, il ringraziamento più grande va ai miei genitori, che mi hanno dato l'opportunità di volare all'estero, anche se questo voleva dire essere lontani da loro. Crescere significa anche trovare il proprio spazio nel mondo, e posso dire che andare a Torino prima e successivamente a Leuven è stato necessario per trovare il mio. Entrambe quelle esperienze facevano parte dei miei sogni, e adesso posso finalmente dire di averli realizzati. Rendere i propri sogni realtà è un privilegio per pochi al giorno d'oggi, e la mia fortuna è stata avere due genitori come voi che mi hanno dato la possibilità di riuscirci. Senza il vostro infinito supporto e incoraggiamento, tutto questo non sarebbe mai stato possibile. So bene che è stato difficile per voi lasciarmi andare, ma ho apprezzato moltissimo il vostro sforzo nel farlo. Come vi ho già detto, anche se dovessi stare lontana per un po', alla fine tornerò sempre a casa da voi, per fare un tuffo insieme al mare e per respirare l'impareggiabile aria di Livorno. Siete la mia certezza. Vi amo, adesso e per sempre.

Giada

Bibliografia

[1] M. Sypabekova, A. Hagemann, A. D. Rho, S. Kim, "Review: 3-Amino propyltriethoxysilane (APTES) Deposition Methods on Oxide Surfaces in Solution and Vapor Phases for Biosensing Applications", *Biosensors*, vol.13, 2023.

[2] R. Bhat and J. Genzer, "Tuning the number density of nanoparticles by multivariant tailoring of attachment points on flat substrates", *Nanotechnology*, 18, 2007.

[3] R. E. G. Van Hal, J. C. T. Eijkel and P. Bergveld, "A general model to describe the electrostatic potential at electrolyte oxide interfaces", *Adv. Colloid Interface Sci.*, 1996.

[4] M. Ponomar, E. Krasnyuk, D. Butylskii, V. Nikonenko, Y. Wang, C. Jiang, T. Xu and N. D. Pismenskaya, "Sessile Drop Method: Critical Analysis and Optimization for Measuring the Contact Angle of an Ion-Exchange Membrane Surface", *Membranes*, 12(8):765, 2022.

[5] A. Moldovan and M. Enachescu, "Wetting Properties at Nanometer Scale", *InTech*, 2015.

[6] L. Abenante, "Incomplete activation and ionization of dopants in Si at room temperature", *Research Article*, 2023.

[7] Sherif M. Sharroush, Yasser S. Abdalla, Ahmed A. Dessouki, and El-Sayed A. El-Badawy, "Subthreshold MOSFET Transistor Amplifier Operation", *IEEE*, 2009.

[8] Biacore AB, "BIACORE Technology Handbook", *GE Healthcare*, 13:14, 1994.

[9] Nico J. de Mol and Marcel J. E. Fischer, "Surface Plasmon Resonance: Methods and Protocols", *GE HumanaPress*, 2010.

[10] Amrita R. Yadav, Rashmi Sriram, Jared A. Carter, Benjamin L. Miller, "Comparative study of solution-phase and vapor-phase deposition of aminosilanes on silicon dioxide surfaces", *Materials Science and Engineering: C*, 35, 283-290, 2014.

[11] S. Fiorilli, P. Rivolo, E. Descrovi, C. Ricciardi, L. Pasquardini, L. Lunelli, L. Vanzetti,C. Pederzolli, B. Onida and E. Garrone, "Vapor-phase self-assembled monolayers of aminosilane on plasma-activated silicon substrates", *Elsevier BV*, 321, 235-241, 2008.

[12] C. Maffeo, J. Yoo, J. Comer, D. B. Wells, B. Luan, and A. Aksimentieva, "Close encounters with DNA", *Phys Condens Matter*, 2014.

[13] V. Gautam, "Dynamically Controlled DNA Tiles: Looking Beyond the Self-assembly of Static Two-dimensional DNA-based Computational Structures", *ResearchGate*, 2017.

[14] Horiba company, "Spectroscopic Ellipsometry: Basic Concepts". [Online], *Horiba scientific website*, url: https://www.horiba.com/ind/scientific/technologies/spectroscopic-ellipsometry/spectroscopic-ellipsometry. [Accessed: 28-Sep-2023].

[15] E. Altamirano-Sánchez, T. Vandeweyer and W. Boullart, "Dry etching patterning requirements for multi-gate devices", *CMOS Nanoelectronics: Innovative Devices, Architectures and Applications*, pp. 29-55, 2012.

[16] R. Vos, C. Rolin, J. Rip, T. Conard, T. Steylaerts, M. V. Cabanilles, K. Levrie, K. Jans and Tim Stakenborg, "Chemical Vapor Deposition of Azidoalkylsilane Monolayer Films", *Langmuir*, 34(4), 1400-1409, 2018.

[17] Robin H. A. Ras, Robert A. Schoonheydt and Cliff T. Johnston, "Relation between s-Polarized and p-Polarized Internal Reflection Spectra: Application for the Spectral Resolution of Perpendicular Vibrational Modes", *J. Phys. Chem*, 111, 8787-879, 2007.

[18] G. Socrates, "Infrared and Raman Characteristic Group Frequencies", *Wiley*, 2001.

[19] M. Gupta, S. Santermans, G. Hellings, L. Lagae, K. Martens and W. Van Roy, "Surface Charge Modulation and Reduction of Non-Linear Electrolytic Screening in FET-Based Biosensing", *IEEE Sens. J.*, vol. 21, no. 4, pp. 4143-4151, 2021.

[20] P. Bergveld, "Thirty years of ISFETOLOGY: What happened in the past 30 years and what may happen in the next 30 years", *Sensors Actuators*, vol. 88, no. 1, pp. 1-20, 2003.

[21] Bor-Ran Li, Chien-WeiChen, Wan-LingYang, Ti-YuLin, Chien-YuanPan, Yit-Tsong Chen, "Biomolecular recognition with a sensitivity-enhanced nanowire transistor biosensor", *Biosensors and Bioelectronics*, vol. 45, pp. 252-259, 2013.

[22] V. Naresh, N. Lee, "A Review on Biosensors and Recent Development of Nanostructured Materials-Enabled Biosensors", *Sensors (Basel)*, 2021.

[23] E. Sudholter, L. De, M. Mescher, and D. Uliie, "Organic Surface Modification of Silicon Nanowire-Based Sensor Devices", *Nanowires - Implementations and Applications. InTech*, 2011.

[24] S. Santermans, "Towards Single-Molecule Sensing with Silicon bioFETs: Modeling and Experiments", *KU Leuven - Faculty of Engineering Science*, 2021.

[25] S. Santermans, F. Schanovsky, M. Gupta, G. Hellings, M. Heyns, W. Van Roy and K. Martens, "The Significance of Nonlinear Screening and the pH Interference Mechanism in Field-Effect Transistor Molecular Sensors", *ACS Sensors*, 2021.

[26] P. Anton van der Merwe, "Surface plasmon resonance", *ResearchGate*, 9:10, 2001.

[27] S. Zafar, C. D'Emic, A. Jagtiani, E. Kratschmer, X. Miao, Yu Zhu, R. Mo, N. Sosa, H. Hamann, G. Shahidi and H. Riel, "Silicon Nanowire Field Effect Transistor Sensors with Minimal Sensor-to-Sensor Variations and Enhanced Sensing Characteristics", *ACS Nano*, 12(7), 6577-6587, 2018.

[28] M. A. Brown, A. Goel and Z. Abbas, Effect of Electrolyte Concentration on the Stern Layer Thickness at a Charged Interface, *Angewandte Chemie*, 2016.

[29] Xuan P. A. Gao, G. Zheng and C. M. Lieber,| "Subthreshold Regime has the Optimal Sensitivity for Nanowire FET Biosensors", *Nano letters*, 10, 547-552, 2010.

[30] ThermoFisher company, "DNA and RNA molecular weights and conversions". [Online], *ThemoFisher website*, url: https://www.thermofisher.com/be/en/home/life-science/protein-biology/protein-biology-learning-center/protein-biology-resource-library/pierce-protein-methods/amine-reactive-crosslinker-chemistry.html. [Accessed: 01-Sep-2023].

[31] S. B. Chiah, X. Zhou, K. Chandrasekaran, K. Y. Lim, L. Chan and S. S. Chu, "Threshold-Voltage-Based Regional Modeling of MOSFETs with Symmetry and Continuity", *NSTI Nanotechnology Conference and Trade Show - NSTI Nanotech*, vol. 2, 2004.

[32] R.E.G. van Hal, J.C.T. Eijkel, P. Bergveld,| "A general model to describe the electrostatic potential at electrolyte oxide interfaces", *Advances in Colloid and Interface Science*, vol. 69, pp. 31-62, 1996.

[33] Anton Paar company, "Zeta potential". [Online], *Anton Paar website*, url: https://wiki.anton-paar.com/it-it/potenziale-zeta. [Accessed: 11-Oct-2023].